21 Brewer M, Gershenson DM, Herzog CE, Mitchell MF, Silva EG, Wharton JT. Outcome and reproductive function after chemotherapy for ovarian dysgerminoma. *J Clin Oncol* 1999; **17**: 2670–5.
22 Thoeny RH, Dockerty MB, Hunt AB, Childs DS Jr. A study of ovarian dysgerminoma with emphasis on the role of radiation therapy. *Surg Gynecol Obstet* 1961; **113**: 692–8.
23 Bendall SC, Stewart MH, Menendez P *et al.* IGF and FGF cooperatively establish the regulatory stem cell niche of pluripotent human cells in vitro. *Nature* 2007; **448**: 1015–U3.
24 Li Y. HOXC8-dependent cadherin 11 expression facilitates breast cancer cell migration through trio and rac. *Genes Cancer* 2011; **2**: 880–8.
25 Nakagawa M, Koyanagi M, Tanabe K *et al.* Generation of induced pluripotent stem cells without Myc from mouse and human fibroblasts. *Nat Biotechnol* 2008; **26**: 101–6.
26 Gordan JD, Thompson CB, Simon MC. HIF and c-Myc: sibling rivals for control of cancer cell metabolism and proliferation. *Cancer Cell* 2007; **12**: 108–13.
27 Seki T, Yuasa S, Fukuda K. Derivation of induced pluripotent stem cells from human peripheral circulating T cells. *Curr Protoc Stem Cell Biol* 2011; 11–14. Chapter 4: Unit4A.3.
28 Buganim Y, Faddah DA, Cheng AW *et al.* Single-cell expression analyses during cellular reprogramming reveal an early stochastic and a late hierarchic phase. *Cell* 2012; **150**: 1209–22.

Supporting Information

Additional supporting information may be found in the online version of this article:

Fig. S1. Expression of embryonic stem cell (ESC) markers in abnormally reprogrammed cells (ARCs).

Fig. S2. Impaired differentiation of abnormally reprogrammed cells (ARCs).

Fig. S3. Expression of c-KIT, CD30, and CD45 in common marmoset dysgerminoma-like cells.

Fig. S4. Colony formation of aorta-gonado-mesonephros fibroblasts by the transduction of OCT3/4, SOX2, KLF4, and c-MYC (OSKM) and OSM.

Fig. S5. Validation of genes showing upregulation in abnormally reprogrammed cells (ARCs) compared to normal induced pluripotent stem (iPS) A cells in microarray analysis.

Fig. S6. Integration of reprogramming genes into the genome of common marmoset dysgerminoma-like cells (CM DGs).

Fig. S7. Fluorescence-activated cell sorter analyses to reveal effects of mitomycin C treatment on common marmoset dysgerminoma-like cell lines.

Fig. S8. Fluorescence-activated cell sorter analyses to reveal effects of cisplatin treatment on common marmoset dysgerminoma-like cell lines.

Fig. S9. Fluorescence-activated cell sorter analyses to reveal effects of irradiation on common marmoset dysgerminoma-like cell lines.

Fig. S10. Knockdown of OCT3/4, SOX2, KLF4, or c-MYC by shRNA in common marmoset dysgerminoma-like cell lines.

Fig. S11. Induction of cell death in common marmoset dysgerminoma-like cells by BGJ398.

Table S1. Lentiviral vector integration sites in common marmoset (CM) dysgerminoma-like cells.

Table S2. Human homologs of candidate tumor suppressors located on chromosome 4q in common marmoset (CM).

Video S1. *In vitro* differentiation assay to assess the ability of abnormally reprogrammed cells to differentiate into cardiomyocytes.

Data S1. Materials and Methods.

FEBS Open Bio 4 (2014) 213–219

FEBS openbio

journal homepage: www.elsevier.com/locate/febsopenbio

Analysis of essential pathways for self-renewal in common marmoset embryonic stem cells

Takenobu Nii [a,1], Tomotoshi Marumoto [a,b,1], Hirotaka Kawano [a], Saori Yamaguchi [a], Jiyuan Liao [a], Michiyo Okada [a], Erika Sasaki [c,d], Yoshie Miura [a], Kenzaburo Tani [a,b,*]

[a] Division of Molecular and Clinical Genetics, Medical Institute of Bioregulation, Kyushu University, 3-1-1, Maidashi, Higashi-ku, Fukuoka 812-8582, Japan
[b] Department of Advanced Molecular and Cell Therapy, Kyushu University Hospital, 3-1-1, Maidashi, Higashi-ku, Fukuoka 812-8582, Japan
[c] Central Institute for Experimental Animals, Kawasaki, Kanagawa 216-0001, Japan
[d] Keio Advanced Research Center, Keio University School of Medicine, Tokyo 160-8582, Japan

ARTICLE INFO

Article history:
Received 21 November 2013
Revised 12 February 2014
Accepted 12 February 2014

Keywords:
Embryonic stem cells
Common marmoset
bFGF
TGFβ
Self-renewal

ABSTRACT

Common marmoset (CM) is widely recognized as a useful non-human primate for disease modeling and preclinical studies. Thus, embryonic stem cells (ESCs) derived from CM have potential as an appropriate cell source to test human regenerative medicine using human ESCs. CM ESCs have been established by us and other groups, and can be cultured *in vitro*. However, the growth factors and downstream pathways for self-renewal of CM ESCs are largely unknown. In this study, we found that basic fibroblast growth factor (bFGF) rather than leukemia inhibitory factor (LIF) promoted CM ESC self-renewal via the activation of phosphatidylinositol-3-kinase (PI3K)-protein kinase B (AKT) pathway on mouse embryonic fibroblast (MEF) feeders. Moreover, bFGF and transforming growth factor β (TGFβ) signaling pathways cooperatively maintained the undifferentiated state of CM ESCs under feeder-free condition. Our findings may improve the culture techniques of CM ESCs and facilitate their use as a preclinical experimental resource for human regenerative medicine.

1. Introduction

Human regenerative medicine, including transplantation of various functional cells differentiated from embryonic stem cells (ESCs) or induced pluripotent stem cells (iPSCs), is considered to have great potential for treating various incurable diseases, and has thus attracted much public attention. However, preclinical studies using animal disease models are required to evaluate the efficacy and safety of ESC/iPSC-derived cells prior to their clinical application. Common marmoset (CM, *Callithrixjacchus*) has recently been recognized as a useful non-human primate for such studies, because of its small size, high reproductive capacity, and genetic similarity to humans [1].

Understanding the molecular mechanisms governing the self-renewal of ESCs is important for the development of technologies to differentiate them into functional cells. Although both human and mouse ESCs are able to self-renew on feeder cells in vitro, their growth factor requirements for self-renewal are different. Basic fibroblast growth factor (bFGF), which activates phosphatidylinositol-3-kinase (PI3K)-protein kinase B (AKT) [2,3] and mitogen-activated protein/extracellular signal-regulated kinase kinase (MEK)-extracellular signal-regulated kinase (ERK) pathways [2–8], and transforming growth factor β (TGFβ) leading to the activation of mothers against decapentaplegic homolog 2/3 (SMAD2/3) [2,6–11], maintain the self-renewal of human ESCs and mouse epiblast stem cells (EpiSCs). Conversely, in mouse ESCs, leukemia inhibitory factor (LIF), which activates janus kinase (JAK)-signal transducer and activator of transcription 3 (STAT3) and PI3K-AKT pathways, is known to play important roles in maintaining self-renewal [12–14].

Abbreviations: AKT, protein kinase B; bFGF, basic fibroblast growth factor; CM, common marmoset; EB, embryoid body; EpiSCs, epiblast stem cells; ERK, extracellular signal-regulated kinase; ESCs, embryonic stem cells; FCM, flow cytometry; iPSCs, induced pluripotent stem cells; JAK, janus kinase; KSR, knockout serum replacement; LIF, leukemia inhibitory factor; MEFs, mouse embryonic fibroblasts; MEK, mitogen-activated protein/extracellular signal-regulated kinase kinase; PI3K, phosphatidylinositol-3-kinase; RT-PCR, reverse transcription-polymerase chain reaction; SMAD2/3, mothers against decapentaplegic homolog 2/3; STAT3, signal transducer and activator of transcription 3; TGFβ, transforming growth factor β

* Corresponding author at: Division of Molecular and Clinical Genetics, Medical Institute of Bioregulation, Kyushu University, 3-1-1, Maidashi, Higashi-ku, Fukuoka 812-8582, Japan. Tel.: +81 92 642 6434; fax: +81 92 642 6444.
E-mail address: taniken@bioreg.kyushu-u.ac.jp (K. Tani).

[1] The first two authors contributed equally to this work.

http://dx.doi.org/10.1016/j.fob.2014.02.007

ESCs derived from CM have been established by us and others [15–17]. However, the growth factors used in the culture medium are different among reports [15,17–21]. Thus, the most appropriate growth factor and its downstream pathway for maintaining the self-renewal of CM ESCs still remain to be determined.

In the present study, we characterized two CM ESC cell lines, Cj11 and CM40, and found that CM ESCs were more similar to human ESCs rather than mouse ESCs in terms of their growth factor requirement and molecular signaling pathways for self-renewal.

2. Materials and methods

2.1. CM ESC culture on mouse embryonic fibroblasts (MEFs)

CM ESC lines, CM40 and Cj11, were maintained in CM ESC medium as described before [15] with or without 1:1000 LIF (Wako, Osaka, Japan), 5 ng/ml bFGF (PeproTech, NJ, USA), 5 μM PD0325901 (MEK inhibitor, Wako) or 10 μM LY294002 (PI3K inhibitor, Santa Cruz Biotechnology, CA, USA). CM40 cell line was established in our laboratory [15], and Cj11 cell line was obtained from WiCell Research Institute [16]. MEFs were prepared from 13.5 dpc embryos from ICR mice (Charles River, Japan) using established procedures [22].

2.2. CM ESC culture under feeder-free conditions

CM40 and Cj11 ESC lines were cultured on Matrigel (BD Biosciences, CA, USA)-coated dishes in Essential 8 medium (Life Technologies, NY, USA) or Essential 6 medium (Life Technologies) with or without 1:1000 LIF (Wako), 100 ng/ml bFGF (PeproTech), 2 ng/ml TGFβ (PeproTech), 5 μM PD0325901 (MEK inhibitor, Wako), 10 μM LY294002 (Santa Cruz Biotechnology).

2.3. CM ESC differentiation

Undifferentiated ESCs were detached from the feeder cells by treatment with 0.25% trypsin (NacalaiTesque, Kyoto, Japan) for 1 min. The collected colonies were processed for embryoid body (EB) formation assay in CM ESC medium on low cell-binding 12-well plates (Nalge Nunc International KK, Japan) for 4 or 8 days. Detailed protocols to differentiate CM ESCs into three germ layers are described in "Supplementary Materials and Methods".

2.4. Immunocytochemistry

Cells were fixed in 4% paraformaldehyde (PFA)/phosphate-buffered saline (PBS) (NacalaiTesque), permeabilized with 0.3% Triton X-100/PBS, blocked with staining buffer (2% fetal bovine serum (FBS)/PBS). The primary antibodies used are shown in Supplementary Table 1. Nuclei were counterstained with DAPI. Images were obtained under a fluorescence microscope (Axiovert 135M; Carl Zeiss, Germany, or BZ-9000; Keyence) and then analyzed by Axiovert software (Carl Zeiss) or BZ-Analyzer software (Keyence).

2.5. Flow cytometry (FCM)

CM ESCs were fixed in 4% PFA/PBS, permeabilized with 0.3% Triton X-100/PBS, blocked with staining buffer (2% FBS/PBS), and then incubated with an anti-OCT3/4 antibody (Santa Cruz Biotechnology, sc-5279 or sc-8628). The cells were detected on a FACSVerse flow cytometer (Becton Dickinson, USA), followed by data analysis using FlowJo software (Tomy Digital Biology, Japan).

2.6. Reverse transcription-polymerase chain reaction (RT-PCR)

Total RNA was isolated using an RNeasy Mini Kit (Qiagen, USA), and cDNA was synthesized using Superscript III reverse transcriptase (Life Technologies). Then PCR was carried out using the synthesized cDNA as templates and gene-specific primers (see Supplemental Table 2). The primers were designed based on different exons to span the intervening intron and avoid amplification of contaminating genomic DNA.

2.7. Western blotting

Cells were incubated on ice with RIPA buffer containing protease inhibitors (Complete Mini, EDTA-free; Roche, Basel, Switzerland) and a phosphatase inhibitor cocktail (NacalaiTesque). The cell lysates were then resolved by SDS-polyacrylamide gel electrophoresis, followed by immunoblotting. The primary antibodies used are shown in Supplementary Table 3. The signals were detected using a LAS3000 (Fujifilm, Japan). Band intensities were measured by ImageJ software (NIH).

2.8. Statistical analysis

Unless otherwise noted, inter-group differences were analyzed using analysis of variance (ANOVA) followed by the Tukey's post-hoc test with GraphPad Prism 5 (GraphPad Software, CA, USA).

3. Results

3.1. bFGF promotes self-renewal of CM ESCs on feeder cells

bFGF and LIF have been reported to be essential for the maintenance of human and mouse ESCs, respectively [3,12–14,23–27], and either or both of these growth factors were considered to be required for the maintenance of CM ESCs. To determine the optimal condition for culturing CM ESCs, we first examined the expression of receptors for bFGF (FGFR1, FGFR2, FGFR3, and FGFR4) and LIF (LIFR and gp130). RT-PCR analysis demonstrated that all of these receptors were expressed in the CM ESCs (Fig. 1A), suggesting that both growth factors play important roles in the biology of CM ESCs.

In culture, ESCs are generally known to spontaneously differentiate. However, the addition of appropriate growth factors inhibits such spontaneous differentiation. To evaluate the effects of bFGF and LIF on the proliferation and differentiation of CM ESCs in vitro, we passaged CM ESCs at a ratio of 1:3 every three days for three passages, and then counted the numbers of undifferentiated OCT3/4$^+$ cells. We found that the proportion of OCT3/4$^+$ cells was unchanged regardless of the addition of bFGF or LIF (Fig. 1B). However, the numbers of OCT3/4$^+$ cells were significantly increased by the addition of bFGF, but not LIF, compared with those of controls cultured without bFGF and LIF (Fig. 1C). Similar results were obtained when the cells were cultured for more than ten passages (Supplementary Fig. S1 and data not shown). The above experiments were performed using CM40 cell line, and similar results were obtained with Cj11 cell line (Supplementary Fig. S2). These results strongly suggest that bFGF promotes the proliferation of CM ESCs rather than maintaining the undifferentiated state of CM ESCs.

3.2. bFGF-PI3K-AKT pathway supports self-renewal of CM ESCs on feeder cells

bFGF and its downstream PI3K-AKT and MEK-ERK pathways are important for the self-renewal of human ESCs [2,3,5,6]. We therefore examined whether these pathways were activated by bFGF for CM ESC self-renewal on feeder cells. CM ESCs were cultured overnight in medium lacking knockout serum replacement (KSR) and any growth factors. Then, we added bFGF (5 ng/ml), and examined the activation of AKT and ERK1/2 in the cells by Western blotting.

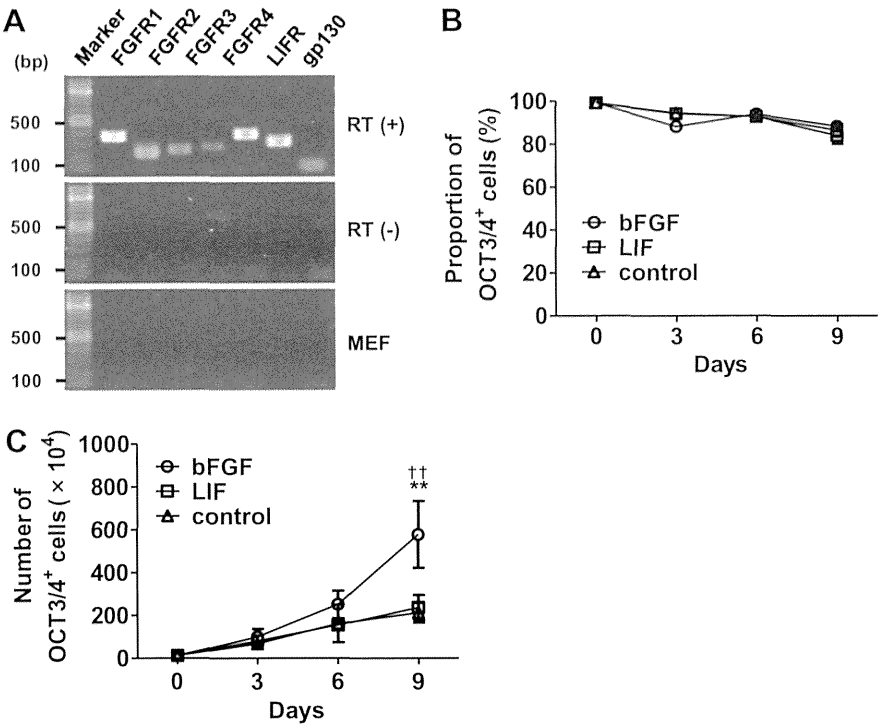

Fig. 1. bFGF promotes self-renewal of CM ESCs in the presence of feeder support. (A) RT-PCR analysis showing the expression of FGFR1, FGFR2, FGFR3, FGFR4, LIFR, and gp130 genes in CM ESCs (CM40). (B) No effect of bFGF on the proportion of OCT3/4$^+$ cells. CM ESCs (CM40; 1.4×10^5) were seeded on mitomycin C (MMC)-treated MEFs and cultured with LIF (open square), bFGF (open circle), or without growth factors (control; open triangle). The percentage of OCT3/4$^+$ cells was determined by FCM. (C) Enhancement of undifferentiated CM ESC growth by bFGF. CM ESCs (CM40; 1.4×10^5) were seeded on mitomycin C (MMC)-treated MEFs and cultured with LIF (open square), bFGF (open circle), or without growth factors (control; open triangle). The number of cells was then counted by trypan blue exclusion. The number of OCT3/4$^+$ cells was determined by multiplying the number of cells by the percentage of OCT3/4$^+$ cells and the passage ratio together. Data are shown as the mean ± SD ($n = 4$). $^{**}P < 0.01$ (bFGF vs. control) and $^{\dagger\dagger}P < 0.01$ (bFGF vs. LIF). Note that all of PCR in (A) was performed with 30 cycles, and no bands were detected for FGFR expression in MEFs in (A), however, they were faintly done when PCR was performed with 40 cycles.

The results showed that the band intensity of phosphorylated AKT was significantly increased after the treatment with bFGF, while that of phosphorylated ERK1/2 was not changed (Fig. 2A and B). These data suggested that PI3K-AKT, but not MEK-ERK, pathway was activated by bFGF in CM ESCs under feeder-dependent culture condition.

Next, to examine whether bFGF-PI3K-AKT pathway plays any roles in the maintenance of self-renewal of CM ESCs, the cells were cultured in medium containing bFGF in the presence or absence of the PI3K inhibitor, LY294002. We found that the proportion of OCT3/4$^+$ cells was maintained at approximately 90% for at least three passages when the cells were cultured without LY294002, whereas it was gradually decreased when the cells were cultured with LY294002 (day0, 96.75 ± 2.83% vs. day9, 57.97 ± 16.76%, Fig. 2C). In addition, OCT3/4$^+$ cell proliferation was inhibited in the presence of LY294002 (day9, bFGF, $7.61 \pm 1.59 \times 10^6$ cells vs. bFGF+LY294002, $2.36 \pm 1.25 \times 10^6$ cells, Fig. 2D). Additionally, even when bFGF was not added, the proportion of OCT3/4$^+$ cells was significantly reduced by the treatment with LY294002 (Fig. 2C), indicating that PI3K-AKT pathway is activated by unknown factors from MEFs and play roles for self-renewal of CM ESCs. Overall, these results strongly suggest that bFGF-PI3K-AKT pathway is essential for the self-renewal of CM ESCs under feeder-dependent culture condition.

To examine the expression of OCT3/4, we used an antibody against amino acids 1–134 of human OCT3/4 (monoclonal OCT3/4 antibody, sc-5279) that was known to be useful for detecting the expression of CM OCT3/4 [28]. And recent study reported that another antibody raised against amino acids 1–19 of human OCT3/4 (polyclonal OCT3/4 antibody, sc-8628) was more useful to detect ESC-specific OCT3/4 [29]. Thus we performed immunocytochemistry and FCM analysis using sc-8628, and obtained the similar results (Supplementary Fig. S3).

3.3. bFGF and TGFβ signaling cooperate to maintain the undifferentiated state of CM ESCs under feeder-free conditions

All of the experiments described above were performed with feeder support. Thus, the various secreted factors including cytokines and adhesion molecules might have affected the results. To examine the dependency of CM ESCs on feeder cells, CM ESCs were cultured on a high or low density of feeder cells, and then the undifferentiated state was examined by immunocytochemistry using an anti-NANOG antibody (Supplementary Fig. S1). We found that CM ESCs on low-density feeder cells lost their expression of NANOG after four passages, whereas those on high-density feeder cells maintained NANOG expression even after ten passages (Supplementary Fig. S1). Therefore, it is conceivable that the self-renewal of CM ESCs is maintained by unknown factors derived from feeder cells.

Chen et al. showed that Essential 8 medium (Dulbecco's modified Eagle's medium/F12 supplemented with L-ascorbic acid-2-phosphate magnesium, insulin, transferrin, sodium selenium, $NaHCO_3$, bFGF, and TGFβ) supports the self-renewal of human ESCs and iPSCs under feeder-free conditions [30]. To clarify the essential growth factors required for maintaining the undifferentiated state of CM ESCs, CM ESCs were cultured under feeder-free condition. We found that CM ESCs could be cultured on Matrigel in Essential 8 medium without feeder support, although they could not be maintained for more than three passages (data not shown). Next, we cultured CM ESCs on Matrigel in Essential 6 medium lacking bFGF and TGFβ overnight, and then the activation of signaling

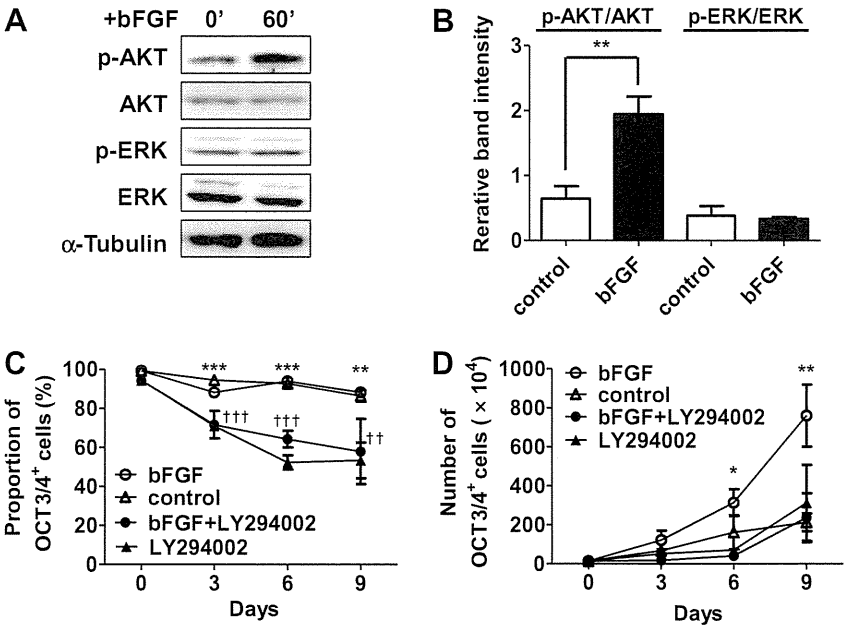

Fig. 2. bFGF-PI3K-AKT pathway supports self-renewal of CM ESCs. (A) Western blot analysis showing the activation of AKT by bFGF in CM ESCs. CM40 cells were starved of bFGF and KSR overnight, and then stimulated with 5 ng/ml of bFGF for the indicated durations. AKT, ERK1/2 and α-Tubulin are shown as loading controls. The relative band intensities of p-AKT/AKT and p-ERK/ERK are shown in (B). Band intensities were measured by ImageJ software. Data are shown as the mean ± SD. The Student's *t*-test was used to test inter-group differences. $^{**}P < 0.01$. (C) Inhibition of self-renewal by LY294002. CM ESCs (CM40; 1.4×10^5) were seeded on MMC-treated MEFs and cultured in medium containing bFGF (open circle), control medium (open triangle), bFGF+LY294002 (closed circle) or LY294002 (closed triangle). The percentage of OCT3/4$^+$ cells was then determined by FCM at the indicated day as shown in (C). The number of live cells was counted by trypan blue exclusion. Growth curves were generated by multiplying the number of live cells by the percentage of OCT3/4$^+$ cells and passage ratio together as shown in (D). Data are shown as the mean ± SD. bFGF, $n = 4$; control, $n = 4$; bFGF+LY294002, $n = 3$; LY294002, $n = 3$; $^{*}P < 0.05$, $^{**}P < 0.01$, and $^{***}P < 0.005$, bFGF vs. control; $^{\dagger\dagger}P < 0.01$ and $^{\dagger\dagger\dagger}P < 0.005$, bFGF+LY294002 or LY294002 vs. control.

pathways known to maintain mouse and human ESCs (bFGF-PI3K-AKT, bFGF-MEK-ERK, TGFβ-SMAD2/3, and LIF-JAK-STAT3 pathways) were analyzed by Western blotting after the addition of bFGF, TGFβ, or LIF to the medium. We found that phosphorylation of AKT and ERK was increased by the addition of bFGF, while it was decreased by the treatment with LY294002 or PD0325901, suggesting that both of AKT and ERK were activated downstream of bFGF under feeder-free condition (Fig. 3A and B). And the addition of TGFβ resulted in an increase of phosphorylated SMAD2/3 (Fig. 3A and B), suggesting that SMAD2/3 was activated downstream of TGFβ. Moreover, the addition of LIF resulted in an increase of phosphorylated STAT3, suggesting that STAT3 was activated downstream of LIF (Supplementary Figs. S4B and D). These results suggested that bFGF-PI3K-AKT, bFGF-MEK-ERK, TGFβ-SMAD2/3 and LIF-JAK-STAT3 pathways known to regulate self-renewal of human or mouse ESCs were activated in CM ESCs under feeder-free condition. It should be noted that ERK was not activated by 5 ng/ml of bFGF that was used for the culture on feeder cells as described in Fig. 2A and B (Supplementary Fig. S4B), but it was remarkably activated by 100 ng/ml of bFGF generally used for feeder-free culture of human ESCs (Fig. 3A and B) [30].

Next, to determine the growth factors maintaining the undifferentiated state of CM ESCs under feeder-free condition, CM ESCs were cultured in the feeder-free system with various combinations of growth factors, followed by analysis of their undifferentiated state morphologically and immunocytochemically. Most of the colonies cultured in Essential 6 medium with bFGF, bFGF+TGFβ, bFGF+LIF, or bFGF+TGFβ+LIF showed a well-packed appearance, and a majority of the cells expressed NANOG (Fig. 3C). In contrast, most of the colonies cultured in Essential 6 medium with TGFβ, LIF, or TGFβ+LIF showed an unpacked appearance, and a majority of the cells did not express NANOG (Fig. 3C). Moreover, NANOG$^+$ and well-packed colonies were found at the highest proportion (98.00 ± 0.88%) when the cells were cultured in the presence of TGFβ+bFGF (Fig. 3D). In addition, almost all of the colonies were positive for OCT3/4, SOX2, SSEA-4, TRA1-60 and TRA1-81 (Supplementary Fig. S3), and these colony forming cells kept the capability of differentiating three lineages (Supplementary Fig. S5). This observation indicates that the addition of both TGFβ and bFGF is the most appropriate growth factor combination for maintenance of the undifferentiated state of CM ESCs under feeder-free condition, which is similar to a characteristic of human ESCs [2,6,9–11].

3.4. CM ESCs show phenotypes similar to those of human ESCs and mouse EpiSCs

Human ESCs and mouse EpiSCs share a number of similar phenotypes as shown in Table 1 [7,8]. CM ESCs formed flattened colonies and expressed NANOG as well as markers for both mouse EpiSCs and human ESCs, such as T, CER1, EOMES, FOXA2, GATA6, and SOX17 (Supplementary Figs. S1 and S6A) [7]. Moreover, bFGF and TGFβ signalings play crucial roles in maintaining the undifferentiated state of human ESCs and mouse EpiSCs [2,7,8,11,30], and the same roles of these signaling pathways were also found in CM ESCs (Fig. 3C and D).

Previous reports have shown that apoptosis of human ESCs and mouse EpiSCs is induced by culturing after complete dissociation [31,32]. Watanabe et al. showed that dissociation-induced apoptosis of human ESCs is suppressed by treatment with the Rho-associated kinase (ROCK) inhibitor Y27632 [33]. To examine whether dissociation-induced apoptosis of human ESCs and mouse EpiSCs was similarly found in CM ESCs, colonies of CM ESCs were dissociated into single cells by trypsinization, and then the cells were plated on Matrigel-coated dishes with or without Y27632. Compared with untreated controls, we found that Y27632-treated CM ESCs produced

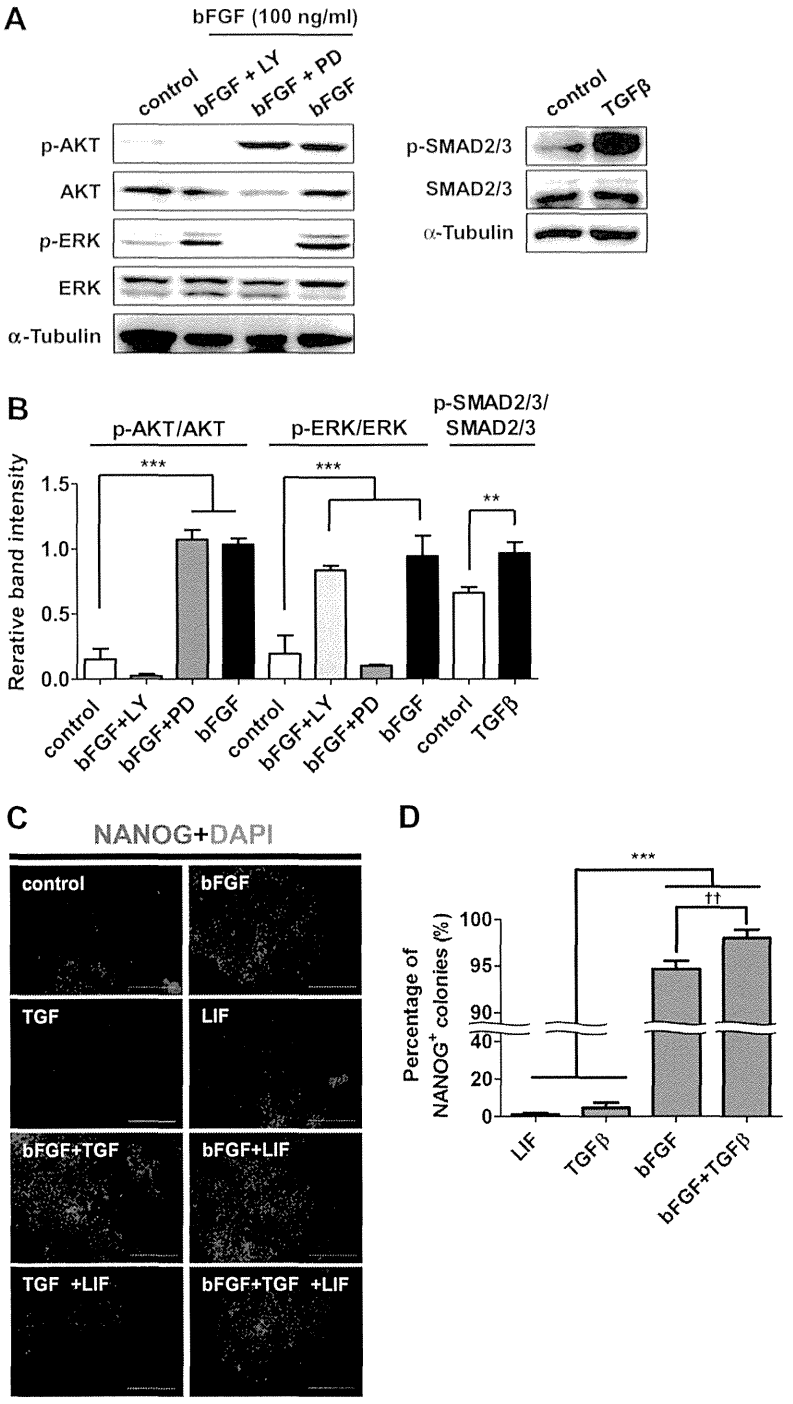

Fig. 3. bFGF and TGFβ maintain the undifferentiated state of CM ESCs under feeder-free conditions. (A) Western blot showing the activation of AKT, ERK1/2 and SMAD2/3 by 100 ng/ml of bFGF or 2 ng/ml of TGFβ for 30 min in CM ESCs. CM40 were starved of growth factors overnight and then pre-treated with LY294002 or PD0325901for 1 h before stimulation with bFGF. AKT, ERK1/2, SMAD2/3, and α-Tubulin are shown as loading controls. The relative band intensities of p-AKT/AKT, p-ERK/ERK and p-SMAD2/3/SMAD2/3 are shown in (B). Band intensities were measured by ImageJ software. Data are shown as the mean±SD. One-way ANOVA followed by the Tukey's post-hoc test was used to test inter-group differences. $^{**}P < 0.01$ and $^{***}P < 0.005$. (C) Immunocytochemical analyses of NANOG expression in CM ESCs (CM40) cultured with various growth factors for 4 days. Merged images of NANOG (red) and nuclei (DAPI; blue) are shown. Scale bars represent 200 μm. NANOG expression in cells cultured without any growth factors is shown as a control. (D) Proportion of NANOG$^+$ colonies. The percentage of NANOG$^+$ colonies cultured with various growth factors was analyzed by immunocytochemistry. For statistical analyses, 300 colonies were examined in each experiment ($n = 3$). Data are shown as the mean ± SD. One-way ANOVA followed by the Tukey's post-hoc test was used to test inter-group differences. $^{***}P < 0.005$. The difference between bFGF- and bFGF+TGFβ-treated cells was statistically analyzed using the Student's t-test. $^{††}P < 0.01$.

significantly more colonies, suggesting that dissociation-induced apoptosis of CM ESCs occurred and was suppressed by Y27632 (Supplementary Figs. S6B and S6C). Thus, we concluded that CM ESCs are similar to human ESCs and mouse EpiSCs.

4. Discussion

Recent advances in the field of basic research for pluripotent stem cells such as the generation of ESCs, iPSCs and stimulus-trig-

Table 1
The characters of mouse EpiSCs and mouse, human and CM ESCs.

Morphology of colony		Mouse ESCs Small, dome	Mouse EpiSCs Large, flat	Human ESCs Large, flat	CM ESCs Large, flat
Growth factor dependency	LIF	+	–	–	–
	bFGF	–	+	+	+
	TGFβ/activin	–	+	+	+
Marker expression	NANOG	+	+	+	+
	OCT3/4	+	+	+	+
	T (brachyury)	–	+	+	+
	CER1	–	+	+	+
	EOMES	–	+	+	+
	FOXA2	–	+	+	+
	GATA6	–	+	+	+
	SOX17	–	+	+	+
Tolerance to single cell dissociation		+	–	–	–
Contribution in chimera		+	–	N/D	N/D

N/D = not determined.

gered acquisition of pluripotency (STAP) cells have given us realistic expectations for human regenerative medicine [22,34–38]. And the need for the development of methods to test new therapeutic approach using such cells is increasing. CM is a useful experimental animal that can suit such needs, and therefore, the characterization of CM ESCs is important. In this study, we investigated essential signaling pathways for the self-renewal of CM ESCs under feeder-dependent and feeder-free culture conditions.

LIF has been widely used to establish and maintain non-human primate ESCs [15,17,18,39–42], although some researchers claim that LIF cannot maintain the self-renewal capacity of these cells [16,41–43]. We found that LIF did not affect the capacity for self-renewal of CM ESCs (Figs. 1 and 3), although it activated the JAK-STAT3 pathway (Supplementary Fig. S3). More extensive studies are needed to further explore the roles of the LIF-JAK-STAT3 pathway in CM ESCs. In our previous report, the expression of LIFR was not found in undifferentiated CM ESCs [15], but it was found in this study after repetitive experiments (Fig. 1A). This discrepancy was considered to be caused by the detection threshold of RT-PCR under different conditions, particularly PCR primers used in our previous report were human LIFR sequence-originated because there were no available marmoset genomic sequence data.

We also found that the self-renewal of CM ESCs cultured on feeder cells was remarkably promoted by bFGF, which is similar to the characteristic of human ESCs (Fig. 1). However, even in the absence of bFGF, most CM ESCs could be maintained in an undifferentiated state by culture on feeder cells, although they showed slower growth compared to those cultured in bFGF containing medium (Fig. 1B and C). This observation indicates that growth factors secreted from feeder cells such as activin, noggin and bFGF, maintain the undifferentiated state of CM ESCs [44,45]. Indeed, CM ESC colonies cultured on low-density feeder cells differentiated within four passages (Supplementary Fig. S1).

Previous studies have demonstrated the critical roles of PI3K-AKT and MEK-ERK pathways in the self-renewal of human ESCs [2–6]. Our results showed that AKT, but not ERK1/2, was activated by the addition of bFGF (5 ng/ml), while ERK1/2 was continuously activated even in the absence of bFGF on feeder support (Fig. 2A). Moreover, inhibition of either MEK-ERK or PI3K-AKT pathways resulted in reduced self-renewal of CM ESCs (Fig. 2 and Supplementary Fig. S7). Therefore, activation of the PI3K-AKT pathway downstream of bFGF as well as the MEK-ERK pathway by unknown mechanisms is required for self-renewal of CM ESCs on feeder support. On the other hand, both AKT and ERK1/2 were activated by the addition of bFGF (100 ng/ml) under feeder-free condition (Fig. 3A and B). And treatment with LY294002 resulted in the elevated expression of endoderm and mesoderm markers, and treatment with PD0325901 caused the reduced expression of these markers, indicating that modulation of these pathways affects the differentiation process in CM ESCs (Supplementary Fig. S8). We are now extensively investigating the effect of these inhibitors on the differentiation process of CM ESCs induced by the treatment with specific cytokines and EB formation assay.

Several studies have demonstrated differences in the mechanisms of ESC self-renewal between mice and humans. Mouse ESCs require LIF for their self-renewal, whereas human ESCs require bFGF and TGFβ. Mouse EpiSCs originating from post-implantation embryos depend on bFGF and TGFβ, and show characteristics similar to those of human ESCs originating from the inner cells mass of blastocysts as shown in Table 1 [7,8,10]. Mouse EpiSCs are therefore considered to be the counterpart of human ESCs. In this study, we demonstrated that CM ESCs were very similar to human ESCs and mouse EpiSCs in terms of their morphology, gene expression, growth factor dependency for self-renewal, and vulnerability to single cell dissociation.

Our findings strongly suggest that CM ESCs are phenotypically similar to human ESCs. Therefore, CM ESCs may facilitate the development of valuable preclinical experimental systems to test new therapeutic modalities for incurable human diseases, particularly in the field of regenerative medicine.

Acknowledgments

We thank Michiko Ushijima for administrative assistance, Yoko Nagai and the members of Tani laboratory for their constructive criticisms and technical support. This work was supported by a grant from the Project for Realization of Regenerative Medicine (K. Tani, 08008010) and KAKENHI (T. Marumoto, 23590465) from the Ministry of Education, Culture, Sports, Science and Technology (MEXT), Japan.

Appendix A. Supplementary data

Supplementary data associated with this article can be found, in the online version, at http://dx.doi.org/10.1016/j.fob.2014.02.007.

References

[1] Hibino, H. et al. (1999) The common marmoset as a target preclinical primate model for cytokine and gene therapy studies. Blood 93, 2839–2848.
[2] Singh, A.M. et al. (2012) Signaling network crosstalk in human pluripotent cells: a Smad2/3-regulated switch that controls the balance between self-renewal and differentiation. Cell Stem Cell 10, 312–326.
[3] Armstrong, L. et al. (2006) The role of PI3K/AKT, MAPK/ERK and NFκβ signalling in the maintenance of human embryonic stem cell pluripotency and

viability highlighted by transcriptional profiling and functional analysis. Hum. Mol. Genet. 15, 1894–1913.
[4] Li, J. et al. (2007) MEK/ERK signaling contributes to the maintenance of human embryonic stem cell self-renewal. Differentiation 75, 299–307.
[5] Na, J., Furue, M.K. and Andrews, P.W. (2010) Inhibition of ERK1/2 prevents neural and mesendodermal differentiation and promotes human embryonic stem cell self-renewal. Stem Cell Res. 5, 157–169.
[6] McLean, A.B. et al. (2007) Activin a efficiently specifies definitive endoderm from human embryonic stem cells only when phosphatidylinositol 3-kinase signaling is suppressed. Stem Cells 25, 29–38.
[7] Tesar, P.J., Chenoweth, J.G., Brook, F.A., Davies, T.J., Evans, E.P., Mack, D.L., Gardner, R.L. and McKay, R.D.G. (2007) New cell lines from mouse epiblast share defining features with human embryonic stem cells. Nature 448, 196–199.
[8] Brons, I.G.M. et al. (2007) Derivation of pluripotent epiblast stem cells from mammalian embryos. Nature 448, 191–195.
[9] James, D., Levine, A.J., Besser, D. and Hemmati-Brivanlou, A. (2005) TGFβ/activin/nodal signaling is necessary for the maintenance of pluripotency in human embryonic stem cells. Development 132, 1273–1282.
[10] Greber, B. et al. (2010) Conserved and divergent roles of FGF signaling in mouse epiblast stem cells and human embryonic stem cells. Cell Stem Cell 6, 215–226.
[11] Vallier, L., Alexander, M. and Pedersen, R.A. (2005) Activin/Nodal and FGF pathways cooperate to maintain pluripotency of human embryonic stem cells. J. Cell Sci. 118, 4495–4509.
[12] Williams, R.L. et al. (1988) Myeloid leukaemia inhibitory factor maintains the developmental potential of embryonic stem cells. Nature 336, 684–687.
[13] Niwa, H., Burdon, T., Chambers, I. and Smith, A. (1998) Self-renewal of pluripotent embryonic stem cells is mediated via activation of STAT3. Genes Dev. 12, 2048–2060.
[14] Takahashi, K., Murakami, M. and Yamanaka, S. (2005) Role of the phosphoinositide 3-kinase pathway in mouse embryonic stem (ES) cells. Biochem. Soc. Trans. 33, 1522.
[15] Sasaki, E. et al. (2005) Establishment of novel embryonic stem cell lines derived from the common marmoset (Callithrix jacchus). Stem Cells 23, 1304–1313.
[16] Thomson, J.A., Kalishman, J., Golos, T.G., Durning, M., Harris, C.P. and Hearn, J.P. (1996) Pluripotent cell lines derived from common marmoset (Callithrix jacchus) blastocysts. Biol. Reprod. 55, 254–259.
[17] Müller, T., Fleischmann, G., Eildermann, K., Matz-Rensing, K., Horn, P.A., Sasaki, E. and Behr, R. (2009) A novel embryonic stem cell line derived from the common marmoset monkey (Callithrix jacchus) exhibiting germ cell-like characteristics. Hum. Reprod. 24, 1359–1372.
[18] Shimada, H. et al. (2012) Efficient derivation of multipotent neural stem/progenitor cells from non-human primate embryonic stem cells. PLoS One 7, e49469.
[19] Maeda, T., Kurita, R., Yokoo, T., Tani, K. and Makino, N. (2011) Telomerase inhibition promotes an initial step of cell differentiation of primate embryonic stem cell. Biochem. Biophys. Res. Commun. 407, 491–494.
[20] Shimoji, K. et al. (2010) G-CSF promotes the proliferation of developing cardiomyocytes in vivo and in derivation from ESCs and iPSCs. Cell Stem Cell 6, 227–237.
[21] Chen, H. et al. (2008) Common marmoset embryonic stem cell can differentiate into cardiomyocytes. Biochem. Biophys. Res. Commun. 369, 801–806.
[22] Takahashi, K., Tanabe, K., Ohnuki, M., Narita, M., Ichisaka, T., Tomoda, K. and Yamanaka, S. (2007) Induction of pluripotent stem cells from adult human fibroblasts by defined factors. Cell 131, 861–872.
[23] Niwa, H., Ogawa, K., Shimosato, D. and Adachi, K. (2009) A parallel circuit of LIF signalling pathways maintains pluripotency of mouse ES cells. Nature 460, 118–122.
[24] Levenstein, M.E., Ludwig, T.E., Xu, R.H., Llanas, R.A., VanDenHeuvel-Kramer, K., Manning, D. and Thomson, J.A. (2006) Basic fibroblast growth factor support of human embryonic stem cell self-renewal. Stem Cells 24, 568–574.
[25] Xu, R.H., Peck, R.M., Li, D.S., Feng, X., Ludwig, T. and Thomson, J.A. (2005) Basic FGF and suppression of BMP signaling sustain undifferentiated proliferation of human ES cells. Nat. Methods 2, 185–190.
[26] Xu, C. et al. (2005) Basic fibroblast growth factor supports undifferentiated human embryonic stem cell growth without conditioned medium. Stem Cells 23, 315–323.
[27] Daheron, L., Opitz, S.J., Zaehres, H., Lensch, W.M., Andrews, P.W., Itskovitz-Eldor, J. and Daley, G.Q. (2004) LIF/STAT3 signaling fails to maintain self-renewal of human embryonic stem cells. Stem Cells 22, 770–778.
[28] Wu, Y., Zhang, Y., Mishra, A., Tardif, S.D. and Hornsby, P.J. (2010) Generation of induced pluripotent stem cells from newborn marmoset skin fibroblasts. Stem Cell Res. 4, 180–188.
[29] Warthemann, R., Eildermann, K., Debowski, K. and Behr, R. (2012) False-positive antibody signals for the pluripotency factor OCT4A (POU5F1) in testis-derived cells may lead to erroneous data and misinterpretations. Mol. Hum. Reprod. 18, 605–612.
[30] Chen, G. et al. (2011) Chemically defined conditions for human iPSC derivation and culture. Nat. Methods 8, 424–429.
[31] Amit, M., Carpenter, M.K., Inokuma, M.S., Chiu, C.-P., Harris, C.P., Waknitz, M.A., Itskovitz-Eldor, J. and Thomson, J.A. (2000) Clonally derived human embryonic stem cell lines maintain pluripotency and proliferative potential for prolonged periods of culture. Dev. Biol. 227, 271–278.
[32] Ohgushi, M. et al. (2010) Molecular pathway and cell state responsible for dissociation-induced apoptosis in human pluripotent stem cells. Cell Stem Cell 7, 225–239.
[33] Watanabe, K. et al. (2007) A ROCK inhibitor permits survival of dissociated human embryonic stem cells. Nat. Biotechnol. 25, 681–686.
[34] Takahashi, K. and Yamanaka, S. (2006) Induction of pluripotent stem cells from mouse embryonic and adult fibroblast cultures by defined factors. Cell 126, 663–676.
[35] Thomson, J.A., Itskovitz-Eldor, J., Shapiro, S.S., Waknitz, M.A., Swiergiel, J.J., Marshall, V.S. and Jones, J.M. (1998) Embryonic stem cell lines derived from human blastocysts. Science 282, 1145–1147.
[36] Evans, M.J. and Kaufman, M.H. (1981) Establishment in culture of pluripotential cells from mouse embryos. Nature 292, 154–156.
[37] Obokata, H., Wakayama, T., Sasai, Y., Kojima, K., Vacanti, M.P., Niwa, H., Yamato, M. and Vacanti, C.A. (2014) Stimulus-triggered fate conversion of somatic cells into pluripotency. Nature 505, 641–647.
[38] Obokata, H. et al. (2014) Bidirectional developmental potential in reprogrammed cells with acquired pluripotency. Nature 505, 676–680.
[39] Shimozawa, N., Nakamura, S., Takahashi, I., Hatori, M. and Sankai, T. (2010) Characterization of a novel embryonic stem cell line from an ICSI-derived blastocyst in the African green monkey. Reproduction 139, 565–573.
[40] Simerly, C.R. et al. (2009) Establishment and characterization of baboon embryonic stem cell lines: An Old World Primate model for regeneration and transplantation research. Stem Cell Res. 2, 178–187.
[41] Suemori, H. et al. (2001) Establishment of embryonic stem cell lines from cynomolgus monkey blastocysts produced by IVF or ICSI. Dev. Dyn. 222, 273–279.
[42] Thomson, J.A., Kalishman, J., Golos, T.G., Durning, M., Harris, C.P., Becker, R.A. and Hearn, J.P. (1995) Isolation of a primate embryonic stem cell line. Proc. Nat. Acad. Sci. 92, 7844–7848.
[43] Mitalipov, S., Kuo, H.C., Byrne, J., Clepper, L., Meisner, L., Johnson, J., Zeier, R. and Wolf, D. (2006) Isolation and characterization of novel rhesus monkey embryonic stem cell lines. Stem Cells 24, 2177–2186.
[44] Wang, G. et al. (2005) Noggin and bFGF cooperate to maintain the pluripotency of human embryonic stem cells in the absence of feeder layers. Biochem. Biophys. Res. Commun. 330, 934–942.
[45] Beattie, G.M., Lopez, A.D., Bucay, N., Hinton, A., Firpo, M.T., King, C.C. and Hayek, A. (2005) Activin A maintains pluripotency of human embryonic stem cells in the absence of feeder layers. Stem Cells 23, 489–495.

Research Article

Cancer Immunology Research

TLR7 Ligand Augments GM-CSF–Initiated Antitumor Immunity through Activation of Plasmacytoid Dendritic Cells

Megumi Narusawa[1], Hiroyuki Inoue[1,2,3], Chika Sakamoto[1], Yumiko Matsumura[1], Atsushi Takahashi[1], Tomoko Inoue[1], Ayumi Watanabe[1], Shohei Miyamoto[1], Yoshie Miura[1], Yasuki Hijikata[3], Yoshihiro Tanaka[3], Makoto Inoue[5], Koichi Takayama[2], Toshihiko Okazaki[4], Mamoru Hasegawa[5], Yoichi Nakanishi[2], and Kenzaburo Tani[1,3]

Abstract

Vaccination with irradiated granulocyte macrophage colony-stimulating factor (GM-CSF)–transduced autologous tumor cells (GVAX) has been shown to induce therapeutic antitumor immunity. However, its effectiveness is limited. We therefore attempted to improve the antitumor effect by identifying little-known key pathways in GM-CSF–sensitized dendritic cells (GM-DC) in tumor-draining lymph nodes (TDLN). We initially confirmed that syngeneic mice subcutaneously injected with poorly immunogenic Lewis lung carcinoma (LLC) cells transduced with Sendai virus encoding GM-CSF (LLC/SeV/GM) remarkably rejected the tumor growth. Using cDNA microarrays, we found that expression levels of type I interferon (IFN)–related genes, predominantly expressed in plasmacytoid DCs (pDC), were significantly upregulated in TDLN-derived GM-DCs and focused on pDCs. Indeed, mouse experiments demonstrated that the effective induction of GM-CSF–induced antitumor immunity observed in immunocompetent mice treated with LLC/SeV/GM cells was significantly attenuated when pDC-depleted or IFN-α receptor knockout ($IFNRA^{-/-}$) mice were used. Importantly, in both LLC and CT26 colon cancer–bearing mice, the combinational use of imiquimod with autologous GVAX therapy overcame the refractoriness to GVAX monotherapy accompanied by tolerability. Mechanistically, mice treated with the combined vaccination displayed increased expression levels of CD86, CD9, and Siglec-H, which correlate with an antitumor phenotype, in pDCs, but decreased the ratio of $CD4^+CD25^+FoxP3^+$ regulatory T cells in TDLNs. Collectively, these findings indicate that the additional use of imiquimod to activate pDCs with type I IFN production, as a positive regulator of T-cell priming, could enhance the immunologic antitumor effects of GVAX therapy, shedding promising light on the understanding and treatment of GM-CSF–based cancer immunotherapy. *Cancer Immunol Res; 2(6); 1–13. ©2014 AACR.*

Introduction

In recent clinical trials of patients with diverse solid cancers, cancer immunotherapy such as therapeutic vaccination with granulocyte macrophage colony-stimulating factor (GM-CSF) gene-transduced tumor vaccines (GVAX), as well as sipuleucel-T (Provenge), the first FDA-approved GM-CSF–based therapeutic dendritic cell (DC) vaccine for prostate cancer, induced antitumor immune responses with tolerability (1–3). However, the efficacy of this therapy alone is not satisfactory, raising an urgent need to improve the antitumor effect of GVAX. Although GM-CSF signaling is essential in conventional DC (cDC) maturation, which leads to effective generation of tumor-associated antigen (TAA)-specific T cells and differentiation, the underlying molecular mechanism of how GM-CSF sensitizes and matures DCs (GM-DC, i.e., GM-CSF–sensitized DCs) to trigger host antitumor immunity remains unclear.

Therefore, in this study, we attempted to improve the antitumor effects of GVAX therapy through the identification of the key cluster genes upregulated in GM-DCs that operate T-cell priming in tumor-draining lymph nodes (TDLN) by conducting a cDNA microarray analysis. We used a syngeneic Lewis lung carcinoma (LLC)–bearing mouse, which exhibited remarkable tumor regression following subcutaneous administration of fusion (F) gene-deleted nontransmissible Sendai virus vector–mediated GM-CSF gene-transduced LLC (LLC/SeV/GM) cells (4). Using this experimental system, the expression microarray analysis elucidated that pathways involving Toll-like receptor 7 (TLR7) and interferon regulatory factor 7 (IRF7), which induce type I interferon (IFN) production in plasmacytoid DCs (pDC; ref. 5), were upregulated in GM-CSF–activated mature DCs. Further activation of this pathway using

Authors' Affiliations: [1]Department of Molecular Genetics, Medical Institute of Bioregulation; [2]Research Institute for Diseases of the Chest, Graduate School of Medical Sciences; [3]Department of Advanced Cell and Molecular Therapy and [4]Center for Clinical and Translational Research, Kyushu University Hospital, Kyushu University, Fukuoka; and [5]DNAVEC Corporation, Tsukuba, Japan

Note: Supplementary data for this article are available at Cancer Immunology Research Online (http://cancerimmunolres.aacrjournals.org/).

Corresponding Author: Kenzaburo Tani, Department of Molecular Genetics, Medical Institute of Bioregulation, Kyushu University, 3-1-1 Maidashi, Higashi-ku, Fukuoka 812-8582, Japan. Phone: 81-92-642-6449; Fax: 81-92-642-6444; E-mail: taniken@bioreg.kyushu-u.ac.jp

doi: 10.1158/2326-6066.CIR-13-0143

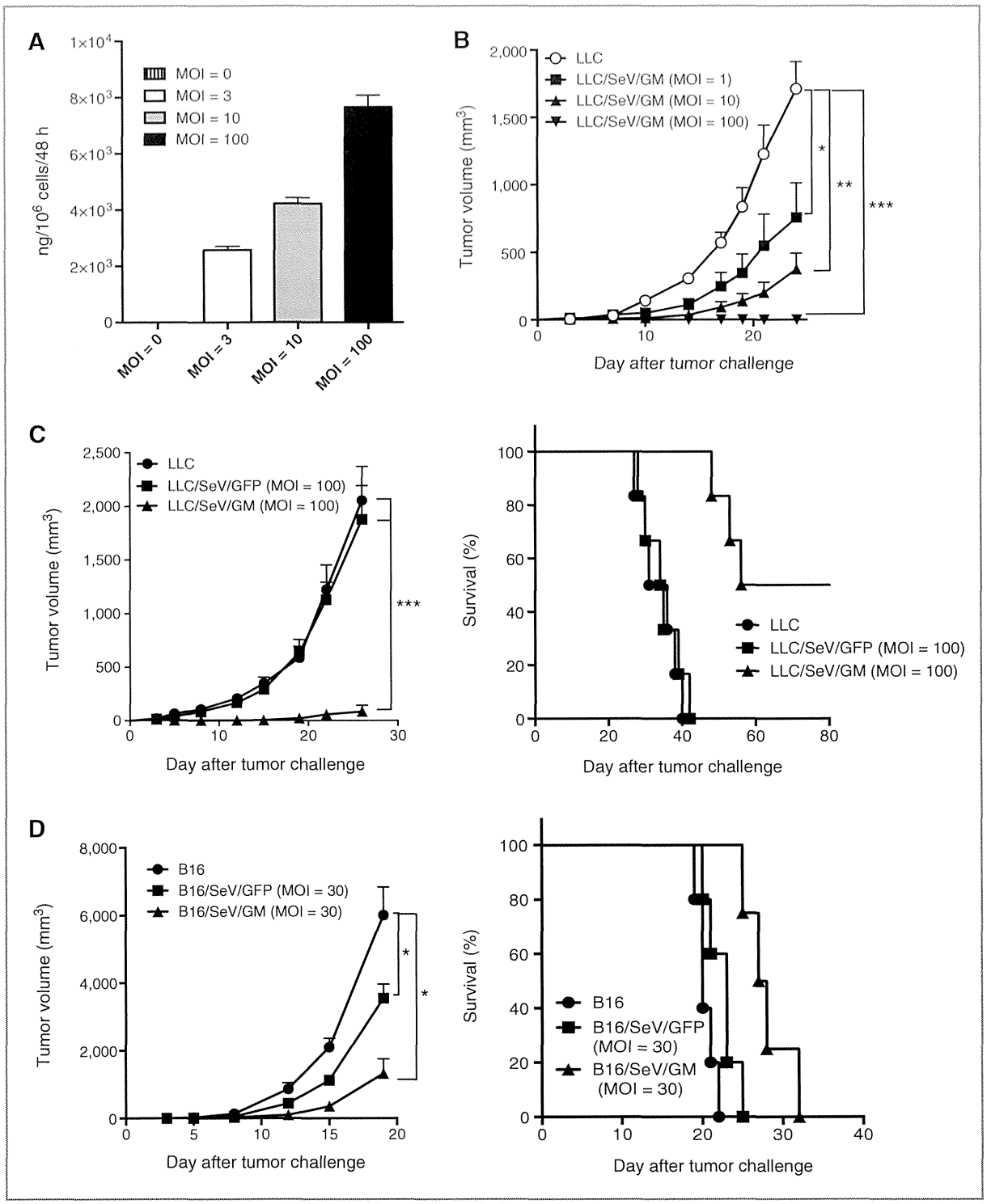

Q13 Figure 1. Tumor development of poorly immunogenic LLC and B16F10 cells modified to produce GM-CSF was markedly inhibited. A, dose-escalation studies to assess GM-CSF production from LLC/SeV/GM cells (MOI = 0, 3, 10, and 100). GM-CSF production levels in the supernatants from the 48-hour culture were measured by ELISA. B and C, tumorigenicity assays using LLC cells. B, a total of 3.0×10^5 LLC and LLC/SeV/GM (MOI of 1, 10, or 100) cells were subcutaneously inoculated into the right flank of C57/BL6N mice ($n = 3$). C, a total of 2.0×10^5 LLC, LLC/SeV/GFP, or LLC/SeV/GM (MOI = 100) cells were inoculated into the right flank of C57/BL6N mice ($n = 6$). (*Continued on the following page.*)

TLR7 agonist enhanced the therapeutic antitumor effects of GVAX therapy using irradiated autologous GM-CSF gene-transduced vaccine cells in both LLC and CT26 tumor-bearing mouse models with augmented pDC activation. These results showed that the combination of GVAX and imiquimod is an effective therapeutic strategy for cancer immunotherapy, and indicates that activated pDCs have a critical role in the GM-CSF–induced induction of antitumor immunity.

Materials and Methods

Mice

Five- to 10-week-old female immunocompetent C57/BL6N and BALB/cN mice were purchased from Charles River Laboratories Japan and housed in the animal maintenance facility at Kyushu University (Fukuoka, Japan). Type I IFN receptor knockout (IFNAR$^{-/-}$) mice were purchased from The Jackson Laboratory. All animal experiments were approved by the Committee of the Ethics on Animal Experiments in the Faculty of Medicine, Kyushu University. Mouse experiments were carried out at least twice to confirm results.

Tumor cell lines

LLC and CT26 cells were purchased from the American Type Culture Collection (ATCC) and passaged for 3 to 4 months after resuscitation. The mouse melanoma cell line (B16F10) was a kind gift from Dr. Shinji Okano (Kyushu University) and was validated as free from *Mycoplasma* infection; no other validations were performed. Both LLC and CT26 cells were validated as free from *Mycoplasma* infection. No other validations were performed; besides, the former were found as free from ectromelia virus. LLC and B16F10 cells were maintained in Dulbecco's Modified Eagle Medium (DMEM; Nakalai Tesque) supplemented with 10% heat-inactivated fetal bovine serum (FBS) and 1% antibiotic mixture (Nakalai Tesque). CT26 was maintained in RPMI-1640 (Nakalai Tesque) supplemented with 10% FBS and 1% antibiotic mixture.

Gene transduction with nontransmissible recombinant Sendai virus vectors

LLC, B16F10, or CT26 cells were infected with nontransmissible Sendai virus vectors encoding green fluorescence protein (GFP) or mouse GM-CSF (SeV/GFP or SeV/GM, respectively), which were prepared by DNAVEC Corp. (6), at the indicated multiplicity of infection (MOI) for 90 minutes (termed as LLC/SeV/GFP, LLC/SeV/GM, B16/SeV/GFP, B16/SeV/GM, or CT26/SeV/GM cells, respectively). They were cultured for 48 hours after viral gene transduction and used for following mouse studies.

In vivo experiments

For tumorigenicity assays, syngeneic C57/BL6N mice were subcutaneously challenged with 2.0×10^5 LLC, LLC/SeV/GFP, or LLC/SeV/GM cells with or without imiquimod (R-837; 50 μg/mouse; Invivogen) or lipopolysaccharide (LPS; 5 μg/mouse; Sigma-Aldrich) resuspended in 100-μL Hanks' Balanced Salt Solution (HBSS; Life Technologies) in the right or left flank. To dissect the role of type I IFN and pDCs in the tumorigenicity assays, IFNAR$^{-/-}$ or pDC-depleted mice were subcutaneously challenged with 2.0×10^5 LLC/SeV/GM cells in the right flank. For therapeutic tumor vaccination assays, LLC/SeV/GFP, LLC/SeV/GM, and CT26/SeV/GM cells were irradiated at 50 Gy and were designated as irLLC/SeV/GFP, irLLC/SeV/GM, and irCT26/SeV/GM cells, respectively. On days 2 and 9 after tumor challenge with parental LLC or CT26 cells, C57/BL6N or BALB/cN mice were subcutaneously vaccinated with the indicated tumor vaccine cells in the opposite flank. Tumor volume was measured every 2 to 4 days and calculated with the following formula: $0.4 \times (\text{largest diameter}) \times (\text{smallest diameter})^2$.

ELISA assay

In vitro expression levels of mouse GM-CSF produced from LLC, LLC/SeV/GFP, or LLC/SeV/GM cells at the MOI and time points were measured using mouse GM-CSF enzyme-linked immunosorbent assay (ELISA) kits (R&D Systems).

Flow cytometric analysis

TDLNs, spleen, and tumor vaccine site (TVS) harvested from the indicated groups of mice ($n = 3$–5) were homogenized and filtered through a 100-μm cell strainer (BD Biosciences). For splenocytes preparation, smashed spleens were treated with ammonium chloride to lyse red blood. For T-cell detection in mixed lymphocyte reaction (MLR) assays, cells were stained with anti-CD4 (RM4.5)–PE (eBioscience), anti-CD3e–APC (145-2C11), and anti-CD8a–PerCP (53-6.7; BioLegend). For phenotypic analyses of DCs in TDLNs, cells were stained with an anti-mouse CD11c Ab [anti-CD11c–APC (N418); BioLegend] in combination with anti-mouse Abs, including anti-B220–PE (RA3-6B2), anti-CD317 (PDCA-1, BST2)–PE (eBio129c; all eBioscience), anti-CD80–PE (16-10A1), anti-CD8a–PerCP, anti-CD86–FITC (GL-1), or anti-CD11b–FITC (M1/70; all BioLegend). For phenotypic analyses of pDCs in TDLNs, cells were stained with either anti-CD317 (PDCA-1, BST2)–PE, anti-PDCA-1–APC (JF05-1C2.4.1; Miltenyi Biotec), or anti-CD11c–PerCPCy5.5 (N418; eBioscience) in combination with anti-mouse Abs, including anti-CD86–FITC, anti-CD9–FITC (MZ3; BioLegend), and anti-Siglec-H–FITC (551.3D3; Miltenyi Biotec). For regulatory T-cell (Treg) detection in TDLNs, cells were permeabilized with Cytofix/Cytoperm kit (BD Biosciences), washed with BD Perm/Wash buffer (BD Biosciences), and stained with anti-CD4, anti-CD25–FITC (PC61.5), and anti-FoxP3–APC (FJK-16s; all eBioscience). Cells were incubated with Abs and analyzed with BD FACSCalibur flow cytometer, CellQuest software (BD Biosciences), and FlowJo software (TreeStar).

(*Continued.*) Significant tumor regression (left) and prolonged survival (right) was shown in mice treated with LLC/SeV/GM cells. D, tumorigenicity assays using B16F10 cells. In total, 1.0×10^5 B16F10, B16/SeV/GFP, or B16/SeV/GM (MOI = 30) cells were inoculated into the right flanks of C57/BL6N mice ($n = 6$). Significant tumor regression (left) and prolonged survival (right) were observed in mice treated with B16/SeV/GM cells. The asterisks indicate statistically significant differences (*, $P < 0.05$; **, $P < 0.01$; ***, $P < 0.001$). Kaplan–Meier survival curves are shown, and mortality was determined by the log-rank test (LLC vs. LLC/SeV/GM and LLC/SeV/GFP vs. LLC/SeV/GM; $P < 0.001$, LLC vs. LLC/SeV/GFP; $P = 0.67$, B16 vs. B16/SeV/GM and B16/SeV/GFP vs. B16/SeV/GM; $P < 0.05$).

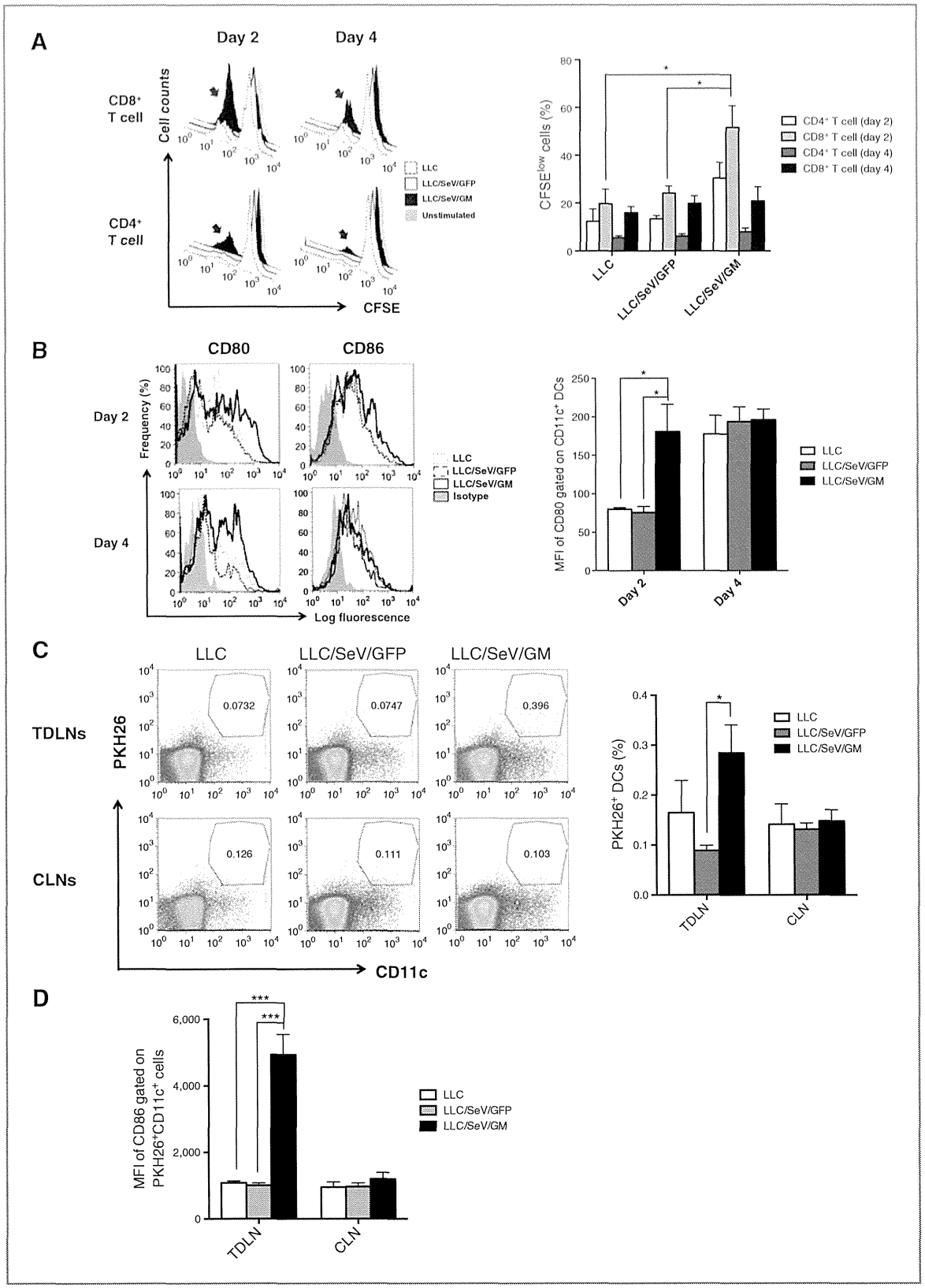
A
Day 2
Day 4
CD8+ T cell
CD4+ T cell
Cell counts
CFSE
LLC
LLC/SeV/GFP
LLC/SeV/GM
Unstimulated
CFSE^low cells (%)
CD4+ T cell (day 2)
CD8+ T cell (day 2)
CD4+ T cell (day 4)
CD8+ T cell (day 4)
B
CD80
CD86
Day 2
Day 4
Frequency (%)
Log fluorescence
Isotype
MFI of CD80 gated on CD11c+ DCs
C
LLC
LLC/SeV/GFP
LLC/SeV/GM
TDLNs
CLNs
PKH26
CD11c
0.0732
0.0747
0.396
0.126
0.111
0.103
PKH26+ DCs (%)
TDLN
CLN
D
MFI of CD86 gated on PKH26+CD11c+ cells

Q16 **Table 1.** Canonical pathways identified by IPA

Pathways	−log (*P* value)	Molecules
Role of pattern recognition receptors in recognition of bacteria and viruses	7.42E+00	OAS1, C3, OAS2, IL6, CCL5, Oas1f, OAS3, IFNA1/IFNA13, TLR2, IFIH1, IRF7, DDX58, TLR7, PIK3R6, EIF2AK2
Pathogenesis of multiple sclerosis	5.33E+00	CXCL10, CXCL9, CCL4, CCL5, CXCL11
Activation of IRF by cytosolic pattern recognition receptors	4.38E+00	DHX58, IFIH1, IRF7, DDX58, ZBP1, STAT2, IL6, IFIT2, IFNA1/IFNA13, ISG15
IFN signaling	3.96E+00	IFIT3, IFIT1, OAS1, MX1, IFI35, STAT2, IFNA1/IFNA13
DC maturation	3.01E+00	FCGR2A, HLA-DMB, IL6, MAPK13, FCGR2B, TREM2, IFNA1/IFNA13, FCGR1A, TLR2, COL1A2, IL1RN, FSCN1, PIK3R6, STAT2
Hepatic fibrosis/hepatic stellate cell activation	2.58E+00	COL1A2, CXCL3, FN1, CXCL9, IGF1, PDGFA, CCL21, CD14, MMP13, CCL5, IL6, IFNA1/IFNA13
Role of hypercytokinemia/hyperchemokinemia in the pathogenesis of influenza	2.49E+00	CXCL10, CCL4, IL1RN, CCL5, IL6, IFNA1/IFNA13
Communication between innate and adaptive immune cells	2.47E+00	CXCL10, TLR2, CCL4, IL1RN, TLR7, CCL5, IL6, IFNA1/IFNA13, Ccl9
Role of tissue factor in cancer	2.45E+00	F10, PDIA2, PIK3R6, HCK, MMP13, F7, LIMK2, MAPK13, FGR, F2
LXR/RXR activation	2.26E+00	APOE, SCD, C3, MSR1 (includes EG:20288), IL1RN, LPL, CLU, CD14, IL6, GC

Allogeneic MLR assays

To prepare $CD11c^+$ DCs as stimulators, on day 2 of the tumorigenicity assay, $CD11c^+$ DCs were purified from TDLNs in mice treated with LLC, LLC/SeV/GFP, or LLC/SeV/GM cells using CD11c MicroBeads (Miltenyi Biotec). To prepare the pDC subset as stimulators, total bone marrow cells harvested from naïve C57/BL6N mice were cultured in RPMI-1640 supplemented with 50 ng/mL murine Fms-related tyrosine kinase 3 ligand (Flt3L; PeproTech) for 8 days and Siglec-H–positive cells (pDCs) were purified using anti-Siglec-H–FITC Ab and anti-FITC MicroBeads (Miltenyi Biotec). Sorted pDCs were then incubated overnight with or without 2.5 μg/mL of imiquimod or 10 ng/mL of murine recombinant GM-CSF (PeproTech). To prepare allogeneic T cells as responders, T cells were sorted from splenocytes harvested from naïve BALB/cN mice using a Pan T-cell isolation kit II (Miltenyi Biotec). A total of 5.0×10^4 responder T cells labeled with 1.0 μmol/L CFSE [5(6)-carboxyfluorescein diacetate N-succinimidylester; Sigma-Aldrich] were cocultured with an equal number of 30 Gy–irradiated $CD11c^+$ DCs. A total of 2.0×10^5 T cells labeled with 2.5 μmol/L of CFSE were cocultured with 4.0×10^4 of pDCs for 5 days. The proliferation rate of the gated $CD3^+$ T-cell fraction was visualized by CFSE dilution.

Detection of DCs that engulfed TAAs

LLC, LLC/SeV/GFP, and LLC/SeV/GM cells were labeled with the PKH26 Red Fluorescent Cell Linker Mini Kit (Sigma-Aldrich), respectively, according to the manufacturer's instruction. On day 2 after they were subcutaneously injected into the right flanks of mice, axillary lymph nodes in both TDLNs and CLNs were harvested, incubated with anti-CD86–FITC and anti-CD11c–APC Abs, and subjected to flow cytometric analysis.

cDNA microarray

Dead cells were excluded from $CD86^+CD11c^+$ DCs using 7-AAD viability dye (Beckman Coulter), which were sorted by FACSAria (BD Biosciences) from TDLNs of mice on day 2 during the tumorigenicity assay. Cells were transferred to RNA later (Life Technologies) to stabilize and protect intact cellular RNA. RNA isolation was performed according to the TRIzol Reagent technical manual (Life Technologies). Total RNA (50 ng) was amplified and labeled using the Agilent Low-Input QuickAmp Labeling Kit, one color (Agilent Technologies). Labeled cRNA was hybridized to Agilent Whole Mouse Genome Oligo DNA microarray (4 × 44 K) v2 (Agilent Technologies). All gene transcription products were hybridized to microarray slides and were scanned by an Agilent scanner.

Figure 2. GM-CSF–sensitized DCs elicited superior capacities to stimulate T-cell proliferation and to mobilize TAA-phagocytosed mature DCs into TDLNs. A, CFSE-labeled allogeneic MLR assay. Irradiated $CD11c^+$DCs from mice treated with indicated tumor challenge were mixed with CFSE-labeled allogeneic T cells. After 3 days of coculture, the proliferation rates of T cells were assessed by flow cytometric analysis. Representative histograms depict CFSE expression of allogeneic $CD4^+CD3^+$ or $CD8^+CD3^+$ T cells (left). Bar graphs, mean + SEM percentage of CFSE-diluted cells/total indicated T cells (right). B, representative histograms depict frequency distributions of MFI of CD80 or CD86 expression in $CD11c^+$ DCs from indicated mouse groups on day 2 or 4 after the tumor challenge (left). Bar graphs, mean + SEM of MFI of CD80 on DCs in TDLNs (right). C, representative dot plots show $PKH26^+CD11c^+$ cells gated by their FSC/SSC profiles in TDLNs or CLNs (left). Bar graphs, mean+SEM of percentage of $CD11c^+PKH26^+$ cells in TDLNs or CLNs (right). D, bar graphs, mean + SEM of MFI of CD86 expression levels in $PKH26^+CD11c^+$ cells (*, $P < 0.05$; ***, $P < 0.001$).

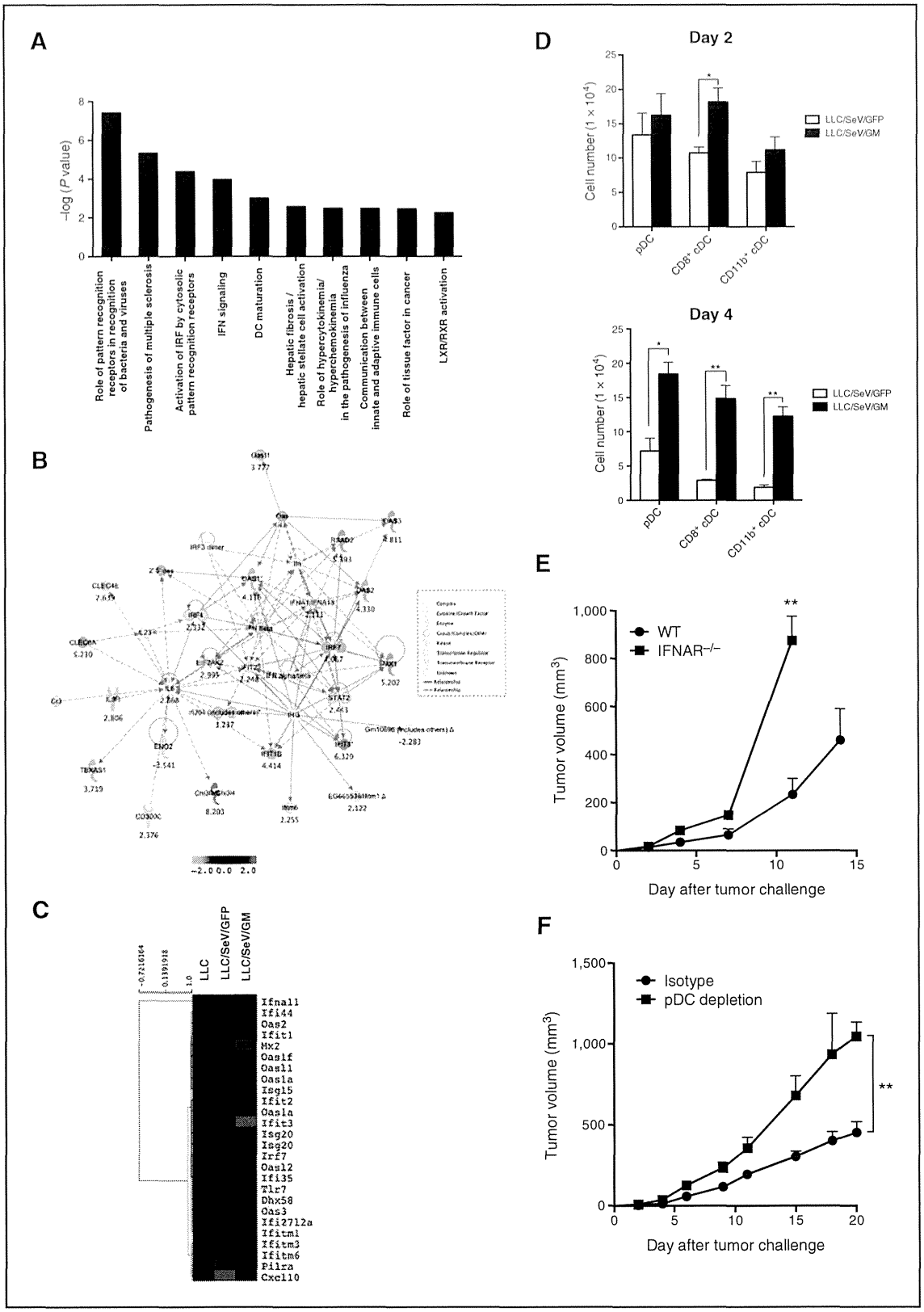
A
−log (P value)
Role of pattern recognition receptors in recognition of bacteria and viruses
Pathogenesis of multiple sclerosis
Activation of IRF by cytosolic pattern recognition receptors
IFN signaling
DC maturation
Hepatic fibrosis / hepatic stellate cell activation
Role of hypercytokinemia/ hyperchemokinemia in the pathogenesis of influenza
Communication between innate and adaptive immune cells
Role of tissue factor in cancer
LXR/RXR activation
B
−2.0 0.0 2.0
C
LLC
LLC/SeV/GFP
LLC/SeV/GM
Ifnal1
Ifi44
Oas2
Ifit1
Mx2
Oas1f
Oasl1
Oas1a
Isg15
Ifit2
Oas1a
Ifit3
Isg20
Isg20
Irf7
Oasl2
Ifi35
Tlr7
Dhx58
Oas3
Ifi2712a
Ifitm1
Ifitm3
Ifitm6
Pilra
Cxcl10
D
Day 2
Cell number (1 × 10⁴)
LLC/SeV/GFP
LLC/SeV/GM
pDC
CD8⁺ cDC
CD11b⁺ cDC
Day 4
E
Tumor volume (mm³)
WT
IFNAR⁻/⁻
Day after tumor challenge
F
Isotype
pDC depletion
Day after tumor challenge

Relative hybridization intensities and background hybridization values were calculated using the Agilent Feature Extraction Software (v9.5.1.1; Agilent Technologies). The raw signal intensities of two samples were $\log_2$-transformed and normalized by a quantile algorithm with the "preprocessCore" library package on Bioconductor software. We used *Z*-scores to compare significant changes in gene expression in each of the three groups (DCs from mice treated with LLC, LLC/SeV/GFP, and LLC/SeV/GM cells). Lists of genes with statistically significant expression in GM-DCs in comparison with GFP-DCs were submitted to Ingenuity Pathway Analysis (IPA; Ingenuity Systems) and analyzed for overrepresented general functions and the resulting networks. Microarray data were deposited in Gene Expression Omnibus (GEO; http://www.ncbi.nlm.nih.gov/geo/; accession number GSE43169).

In vivo depletion experiments

To deplete pDCs, mice were injected intraperitoneally with 100 μg of anti-PDCA-1 mAb (JF05-1C2.4.1; Miltenyi Biotec) or control Ab (rat IgG; Jackson Immunoresearch), as previously described (7). Effective depletion of PDCA-1^+ cells was confirmed by flow cytometric analysis (Supplementary Fig. S1). $CD4^+$ T or $CD8^+$ T cells were depleted by using GK1.5 or 2.43 mAbs, as previously described (8). Briefly, mice received intraperitoneal injections of anti-mouse GK1.5 mAb, anti-mouse 2.43 mAb (50 μg/mouse), or control Ab at 6, 4, and 2 days before tumor challenge, and once every 3 days thereafter. Effective depletion of $CD4^+$ and $CD8^+$ T cells was confirmed by flow cytometric analysis (data not shown).

Results

Production of GM-CSF from LLC and B16F10 cells remarkably impaired the tumorigenicity

To test the possibility that substantial secretion of GM-CSF from syngeneic mouse cancer cells facilitates the development of antitumor immune responses, we used recombinant nontransmissible Sendai virus vectors expressing GM-CSF (SeV/GM) at various MOI. Abundant GM-CSF production from the infected LLC (LLC/SeV/GM) cells was observed and was MOI dependent (Fig. 1A). The proliferation rate of LLC cells was not affected by transduction with SeV/GM, as previously described (6). We next performed tumorigenicity assays in which each LLC and LLC/SeV/GM cells (MOI = 1, 10, and 100) were subcutaneously injected into the left flank of syngeneic mice. All mice treated with LLC/SeV/GM cells exhibited significant suppression of the tumor outgrowth in an MOI-dependent manner (Fig. 1B). We thus determined MOI = 100 for gene transduction as an optimized infection dose. Notably, mice treated with LLC/SeV/GM cells significantly suppressed tumor growth and prolonged the survival of mice, compared with control groups ($P < 0.001$; Fig. 1C). Similar suppression of tumor growth and prolongation of mouse survival were observed when SeV/GM-infected B16F10 melanoma cells were injected to C57BL/6N mice (Fig. 1D).

Increased ability of GM-CSF–sensitized DCs to stimulate T-cell proliferation, accelerate their maturation, and deliver phagocytosed TAAs in TDLNs

To determine a putative phase when GM-CSF–sensitized DCs from TDLNs of mice treated with LLC/SeV/GM cells (GM-DCs) effectively prime naïve T cells, we performed allogeneic MLR assays. GM-DCs exhibited a significantly marked response on day 2 compared with DCs from mice treated with LLC/SeV/GFP cells (GFP-DCs), and stimulated the proliferation of allogeneic $CD3^+CD4^+$ T and $CD3^+CD8^+$ T cells (Fig. 2A). Furthermore, GM-DCs harvested on day 2 elicited higher expression levels of costimulatory maturation markers CD80 and CD86 than those from control mice (Fig. 2B), suggesting that day 2 could be the putative phase to mount optimum immunologic responses by GM-DCs. To explore the migratory capacity of GM-DCs that phagocytosed TAAs at the tumor injection site, we inoculated PKH26-labeled LLC, LLC/SeV/GFP, or LLC/SeV/GM cells into the right flank of mice, and evaluated $PKH26^+$ DC numbers in both TDLNs and contralateral LNs (CLN). The frequencies of $PKH26^+$ DCs in TDLNs, but not CLNs, harvested from mice treated with LLC/SeV/GM cells were significantly increased, indicating that GM-CSF production potentiated the migration of PKH26-labeled LLC cells (TAA)–phagocytosed DCs from the tumor injection site into TDLNs ($P < 0.05$; Fig. 2C). $PKH26^+$ GM-DCs derived from TDLNs, but not from CLNs, showed significantly higher CD86 expression than controls ($P < 0.001$; Fig. 2D).

cDNA microarray analysis revealed the involvement of type I IFN–related pathways in GM-CSF–induced antitumor immunity

On the basis of the aforementioned results, we determined day 2 to be an adequate time point for the peak in T-cell priming by TAA-phagocytosed $CD86^+$ DCs. To address the important factor of DCs/T-cell priming, we isolated $CD86^+$ DCs from mice treated with LLC/SeV/GM cells and control groups, and compared the comprehensive gene expression patterns of isolated $CD86^+$ DCs in TDLNs. After normalization of microarray data and statistical analysis, 1,318 genes were

Figure 3. Transcriptome analysis suggested the involvement of type I IFN–related pathways in GM-DCs during GM-CSF–induced antitumor immunity. A, total RNA was isolated from $CD86^+$ DCs in TDLNs from mice inoculated with LLC, LLC/SeV/GFP, or LLC/SeV/GM cells at 2 days after the tumor challenge and subjected to cDNA microarray. The top 10 canonical pathways significantly upregulated in GM-DCs, in comparison with those in GFP-DCs, by which a right-tailed Fisher exact test was calculated using the entire dataset. B, IPA was performed using the type I IFN pathway–related genes from the original commonly regulated probes differentially expressed between GFP-DCs and GM-DCs. Differentially expressed genes are indicated in red and green, representing up- and downregulation induced by GM-CSF activation, respectively. A high degree of gene regulation is indicated by bold colored genes. Direct or indirect associations with the differentially expressed genes indicated by no color were not found to be significantly different in this assessment. Positive regulatory interactions are depicted by solid arrows (direct interactions) or dashed arrows (indirect interactions). C, heatmap based on type I IFN pathway–related genes that were differentially expressed in $CD86^+$ DCs in TDLNs from indicated mouse groups. D, cell numbers of DC subsets (pDC, $CD8^+$ cDCs, and $CD11b^+$ cDC) in TDLNs at day 2 (top) and 4 (bottom) after the respective tumor challenge were comparatively quantified (*, $P < 0.05$; **, $P < 0.01$). E and F, representative tumor growth curves observed in $IFNAR^{-/-}$ (E) or pDC-depleted (F) mice (*, $P < 0.05$; **, $P < 0.01$).

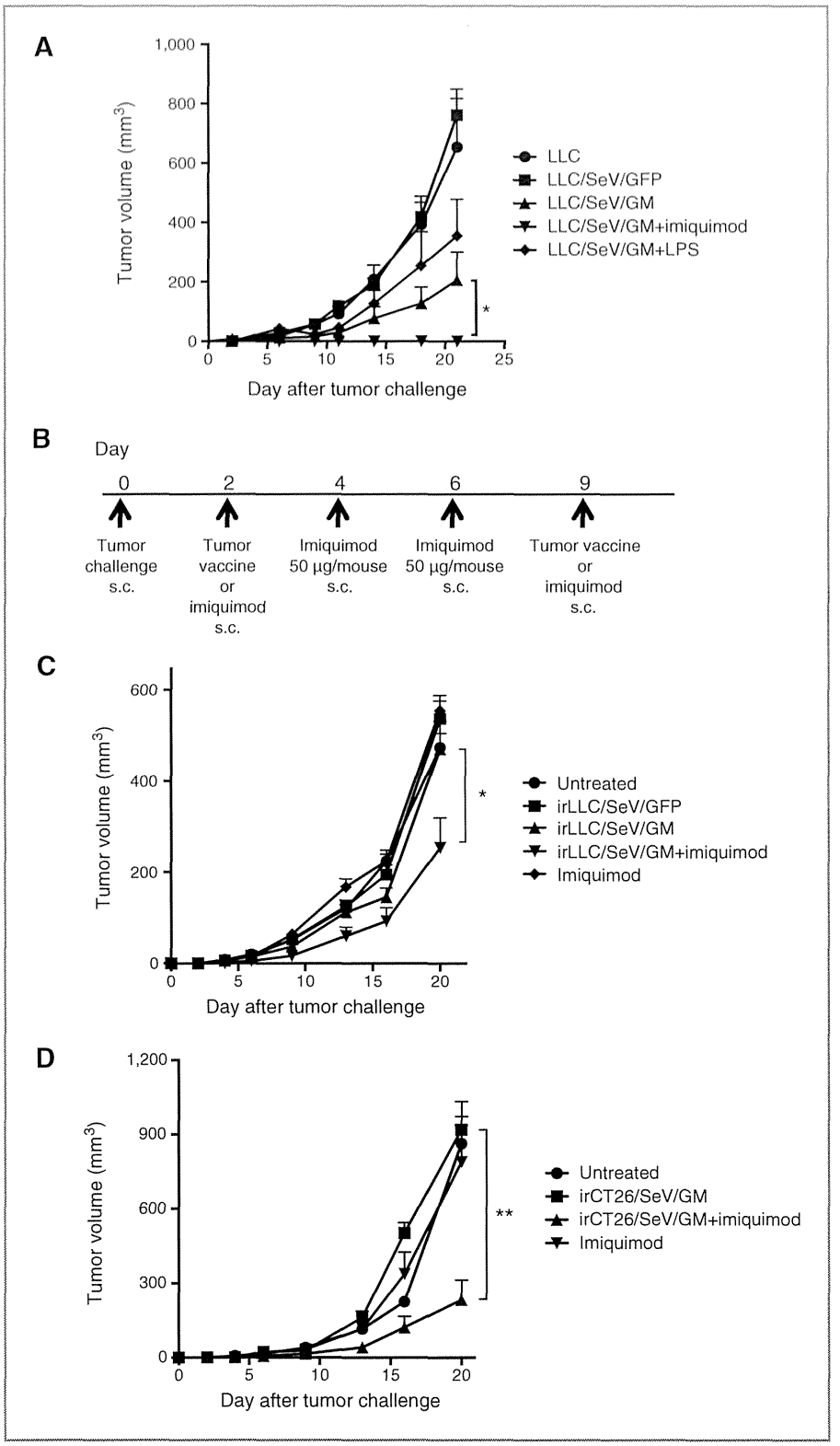

Figure 4. Combined imiquimod and irLLC/SeV/GM cells exert significant therapeutic antitumor effects compared with irLLC/SeV/GM cells alone. A, a total of 2.0×10^5 LLC and LLC/SeV/GM cells with or without LPS or imiquimod were subcutaneously inoculated into the right flanks of C57/BL6N mice. Bar graphs, mean + SEM of tumor volumes. Combined data from two independent experiments with similar results are shown (*, $P < 0.05$). B, schematic diagram of the experimental protocol of therapeutic GM-CSF–based tumor vaccination. Briefly, 2.0×10^5 LLC cells or 3.0×10^5 CT26 cells were inoculated subcutaneously to C57/BL6N or BALB/cN mice. LLC-bearing mice were divided into the following groups: untreated, imiquimod alone, irLLC/SeV/GFP, irLLC/SeV/GM, or irLLC/SeV/GM cells plus imiquimod. CT26-bearing mice were divided into the following groups: untreated, imiquimod alone, irCT26/SeV/GM or irCT26/SeV/GM cells plus imiquimod. On days 2 and 9, mice were inoculated subcutaneously with the indicated vaccine cells. For imiquimod administration, mice were subcutaneously inoculated with imiquimod on days 2, 4, 6, and 9. Represented are tumor growth curves observed in either LLC- (C) or CT26-bearing (D) mice (*, $P < 0.05$; **, $P < 0.01$).

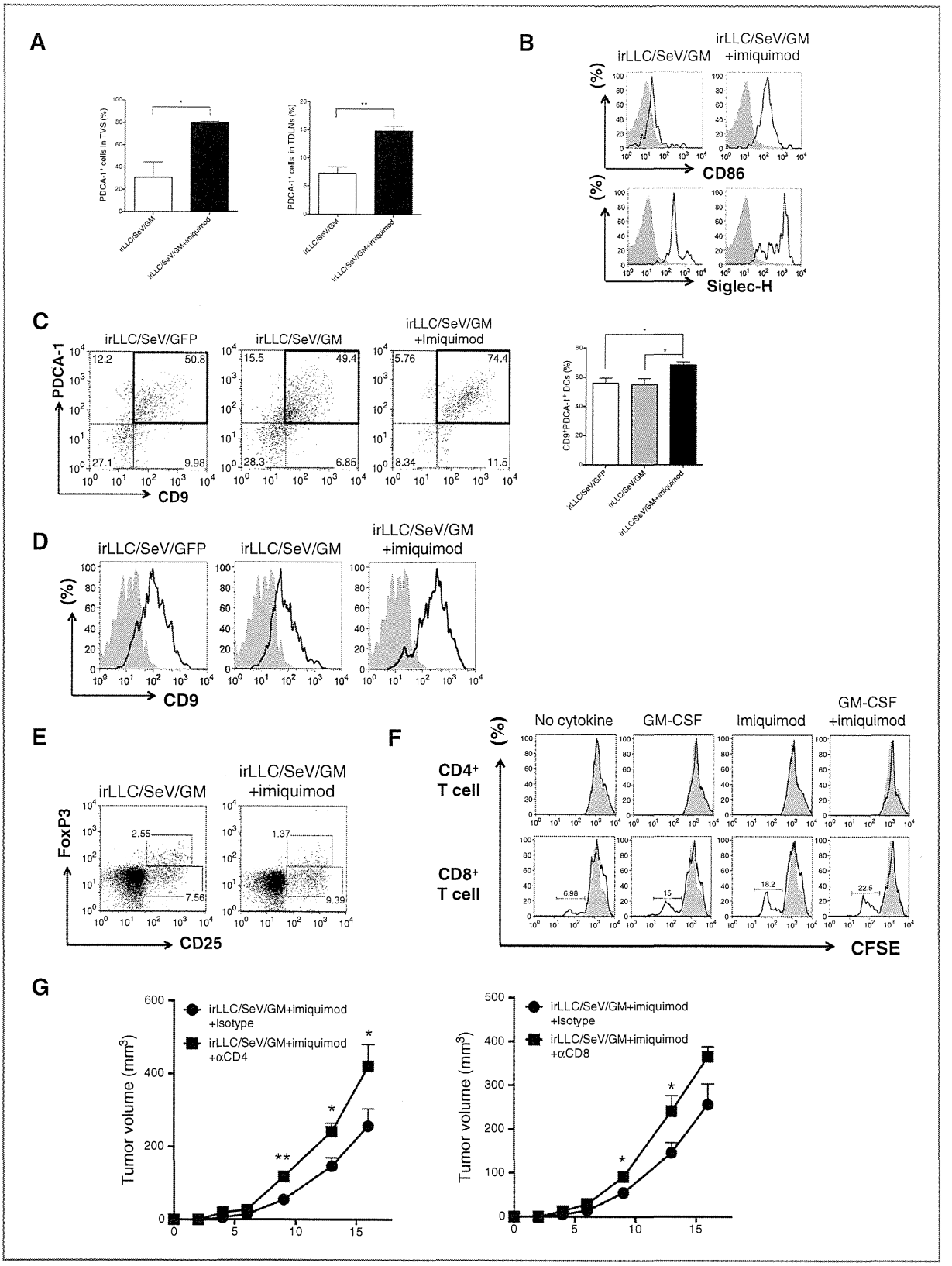
A
PDCA-1+ cells in TVS (%)
PDCA-1+ cells in TDLNs (%)
irLLC/SeV/GM
irLLC/SeV/GM+imiquimod
B
irLLC/SeV/GM
irLLC/SeV/GM +imiquimod
(%)
CD86
Siglec-H
C
irLLC/SeV/GFP
irLLC/SeV/GM
irLLC/SeV/GM +Imiquimod
PDCA-1
CD9
12.2
50.8
27.1
9.98
15.5
49.4
28.3
6.85
5.76
74.4
8.34
11.5
CD9+PDCA-1+ DCs (%)
D
irLLC/SeV/GFP
irLLC/SeV/GM
irLLC/SeV/GM +imiquimod
(%)
CD9
E
irLLC/SeV/GM
irLLC/SeV/GM +imiquimod
FoxP3
CD25
2.55
7.56
1.37
9.39
F
No cytokine
GM-CSF
Imiquimod
GM-CSF +imiquimod
(%)
CD4+ T cell
CD8+ T cell
6.98
15
18.2
22.5
CFSE
G
Tumor volume (mm3)
irLLC/SeV/GM+imiquimod +Isotype
irLLC/SeV/GM+imiquimod +αCD4
irLLC/SeV/GM+imiquimod +αCD8

found to be differentially expressed between GM-DCs and GFP-DCs with statistical significance (upregulated genes; *Z*-score ≥ 2 and ratio >1.5, downregulated genes; *Z*-score ≤ -2 and ratio <0.66; data not shown). A list of the genes significantly upregulated in the top 10 canonical pathways in $CD86^+$ GM-DCs in comparison with $CD86^+$ GFP-DCs is shown in Table 1. As expected, these genes composed immunologic response–related pathways (Fig. 3A). Among the activated pathways triggered by GM-CSF, we focused on the following representative molecules: IRF7, Oas3 (2′-5′-oligoadenylate synthetase 3), and TLR7, which constitute the type I IFN (IFN-α/IFN-β)–associated pathways (Fig. 3B and C; refs. 5, 9). Microarray results for the expression levels of IRF7 and Oas3 were validated by performing qRT-PCR (Supplementary Fig. S2). As pDCs provoke initial defensive antiviral responses by type I IFN production and are the main producers of type I IFNs (10), we speculated that pDCs could be positively involved in the induction of effective GM-CSF–sensitized DCs/T-cell priming (11). Indeed, the number of pDCs, $CD11b^+$ cDCs, and $CD8^+$ cDCs subsets from total GM-DCs from TDLNs harvested on days 2 and 4 were greater than the equivalent subsets from total GFP-DCs (Fig. 3D). Furthermore, the results of *in vivo* experiments using IFN-α receptor knockout ($IFNAR^{-/-}$) mice demonstrated that $IFNAR^{-/-}$ mice inoculated with LLC/SeV/GM cells significantly abrogated the impairment of tumorigenicity seen in the corresponding wild-type (WT) mice (Fig. 3E). Importantly, similar results were also obtained when pDC-depleted mice were used (Fig. 3F). These results collectively demonstrate the positive role of type I IFN–producing pDCs in the induction of GM-CSF–mediated antitumor immunity.

Combination of TLR7 ligand and GM-CSF–secreting LLC cells enhanced the induction of antitumor immunity in both tumorigenicity and therapeutic vaccination models

TLR7-dependent type I IFN pathways are activated by binding with their corresponding ligand, imiquimod (12). To examine the impact of the TLR7-mediated activation of type I IFN–related pathways primarily in pDCs on GM-CSF–induced antitumor immunity, we performed a gain-of-function assay by evaluating the tumorigenicity of LLC/SeV/GM cells with or without imiquimod or TLR4 ligand, LPS, as an irrelevant control. Mice treated with LLC/SeV/GM cells combined with imiquimod significantly suppressed tumor development accompanied with complete tumor regression in all mice tested ($P < 0.05$). Conversely, mice treated with LLC/SeV/GM cells combined with LPS rather attenuated the GM-CSF–induced antitumor effects (Fig. 4A) and exhibited no significant changes in body weight (Supplementary Fig. S3). We next attempted to translate these findings into a tumor vaccination therapy by adding imiquimod to the subcutaneous administration of irradiated LLC/SeV/GM (irLLC/SeV/GM) cells to investigate the synergistic effect. Notably, mice treated with combined imiquimod and irLLC/SeV/GM cells elicited a significantly marked suppression of tumor growth of preestablished LLC cells, whereas control mice treated with irLLC/SeV/GM cells or imiquimod alone manifested negligible antitumor effects ($P < 0.05$; Fig. 4B and C). Similarly, mice vaccinated with irradiated GM-CSF gene-transduced (MOI = 100) CT26 colon cancer cells in combination with imiquimod significantly suppressed tumor development ($P < 0.01$; Fig. 4D).

Admixed use of TLR7 ligand in combination with GVAX therapy induced pDC activation leading to generation of T-cell–mediated antitumor immunity

To elucidate the effect of imiquimod on GM-CSF–induced initial immune responses, we performed phenotypic immunoanalyses. At 6 hours after the first tumor vaccination, mice treated with irLLC/SeV/GM cells plus imiquimod showed a significantly higher frequency and number of cells expressing PDCA-1, a pDC-specific marker, than control mice in both TVSs and TDLNs (Fig. 5A and Supplementary Fig. S4). Furthermore, pDCs ($CD11c^+PDCA\text{-}1^+$ cells) derived from mice treated with irLLC/SeV/GM cells plus imiquimod expressed increased levels of CD86 and sialic acid binding Ig-like lectin (Siglec)-H, a functional pDC-specific receptor (Fig. 5B; ref. 13), accompanied with significantly higher levels of serum IFN-α (Supplementary Fig. S5). Because $CD9^+$ pDCs stimulated with TLR agonists induced higher amounts of IFN-α and provoked protective T-cell–mediated antitumor immunity (14), we compared CD9 expression levels on pDC subsets. Mice treated with irLLC/SeV/GM cells plus imiquimod had significantly increased frequency and MFI of $CD9^+PDCA1^+CD11c^+$ pDCs in TDLNs (Fig. 5C and D). However, the frequency of $CD4^+$ $CD25^+FoxP3^+$ Tregs was decreased in TDLNs from mice treated with irLLC/SeV/GM cells and imiquimod, whereas the frequency of $CD4^+CD25^+FoxP3^-$ T cells was increased in mice treated with combined therapy (Fig. 5E). To investigate the effect of imiquimod and GM-CSF on the T-cell proliferation capacity of pDCs, we performed an allogeneic MLR assay. pDCs stimulated with GM-CSF and imiquimod elicited the most pronounced proliferative activity of $CD8^+$ T cells, but not $CD4^+$ T cells, when compared with controls (Fig. 5F). Moreover, the

Figure 5. Mice vaccinated with combined irLLC/SeV/GM cells and imiquimod augmented the recruitment of activated pDCs in TDLNs. A, at 6 hours after the first tumor vaccination, infiltrating lymphocytes in TVSs or TDLNs were harvested from indicated mouse groups. Bar graphs, mean + SEM of frequency of $PDCA\text{-}1^+$ cells gated on FSC/SSC profiles. B, histograms represent expression levels of Siglec-H or CD86 expression on $CD11c^+PDCA\text{-}1^+$ cells (pDCs) in TDLNs from indicated mouse groups (tinted light gray, isotype control; bold line, anti-CD86 or anti-Siglec-H Ab. C, on day 12, TDLNs were harvested from mice treated with irLLC/SeV/GFP, irLLC/SeV/GM, or irLLC/SeV/GM cells plus imiquimod ($n = 3$). Representative dot plots depict CD9 and PDCA-1 expression gated on $CD11c^+$ cells in TDLNs (left). Bar graphs, mean + SEM of frequency of $CD9^+PDCA\text{-}1^+$ cells on DCs (*, $P < 0.05$; right). D, histograms depict MFI representing CD9 expression levels on $PDCA\text{-}1^+CD11c^+$ subpopulations in TDLNs (tinted light gray, isotype control; bold line, anti-CD9 Ab). E, representative dot plots illustrate CD25 and FoxP3 expression gated on $CD4^+$ T cells in TDLNs from indicated mouse groups. F, CFSE-labeled allogeneic MLR assay. Bone marrow–derived pDCs treated with GM-CSF or imiquimod or in combination with GM-CSF plus imiquimod were mixed with CFSE-labeled T cells. Representative histograms show CFSE expression of allogeneic $CD4^+CD3^+$ or $CD8^+CD3^+$ T cells stimulated by the indicated pDCs. G, tumor growth curves in $CD4^+$ T-cell (left)– or $CD8^+$ T-cell (right)–depleted mice treated with irLLC/SeV/GM cells plus imiquimod (*, $P < 0.05$; **, $P < 0.01$).

synergistic therapeutic efficacy of irLLC/SeV/GM cells and imiquimod was significantly inhibited when the corresponding mice were depleted of $CD4^+$ or $CD8^+$ T cells (Fig. 5G).

Discussion

This study demonstrates that SeV/dF-mediated exogenous expression of GM-CSF caused poor growth of cancer cells in syngeneic mice, concomitant with an early appearance of mature DCs in TDLNs. We used SeV/dF vectors for the gene transduction of vaccine cells because they have relatively higher capacities in terms of gene transduction, induction of antitumor immunity, and safety (6, 15). Expression microarray analyses of the GM-CSF–sensitized $CD86^+$ DCs revealed increased expression of the TLR7–IRF7 pathway components, which induce type I IFN production in pDCs (5). Furthermore, the addition of imiquimod was found to be an effective potential approach to improve the antitumor effects of GVAX therapy (Fig. 4).

As LLC cells have been considered as poorly immunogenic in lung cancer (16), it was surprising that tumor challenge with LLC/SeV/GM cells markedly impaired its tumorigenicity with complete tumor disappearance in half of the mice tested (Fig. 1). In addition, mice that received prophylactic vaccination with irLLC/SeV/GM cells also significantly inhibited subsequent tumor challenge with LLC cells (Supplementary Fig. S6). However, therapeutic vaccination using irLLC/SeV/GM cells alone failed to exert significant antitumor immunity (Fig. 4C). We, therefore, attempted to potentiate the therapeutic antitumor effects of irLLC/SeV/GM cells through scrutinizing the gene expression signature of GM-CSF–sensitized DCs in TDLNs from mice that strongly rejected the tumor challenge with LLC/SeV/GM cells. We confirmed that GM-CSF facilitated the maturation of DCs into antigen-presenting cells (APC) with enhanced ability to prime naïve T cells to proliferate, and to increase expression of CD80, CD86, MHC class I, MHC class II, and CD40 (Fig. 2B and Supplementary Fig. S7), consistent with previous finding that GM-CSF promotes DCs maturation and differentiation (17). Herein, transcriptome analyses revealed that GM-CSF also modulated signal transduction in pDCs by upregulation of the TLR7–IRF7 pathway related to type I IFN production (Fig. 3), consistent with a previous report in which GM-CSF stimulation upregulated TLR7 expression in mouse immune cells (18). Our observation that the pDC subset was markedly increased in GM-DCs from TDLNs was unexpected, as the GM-CSF receptor is mainly expressed on $CD34^+$ progenitor cells and myeloid cells (19, 20), and GM-CSF administration preferentially expands $CD11b^+$ cDC (21, 22) and inhibits pDC differentiation (23). However, recent studies showing that pDC precursors differentiated to $CD11b^+$MHC II^{high} cDCs by GM-CSF stimulation (24), the identification of GM-CSF as a novel activator of pDCs revealed by systematic analysis of cytokine receptors (25), may explain the increase of GM-CSF–sensitized pDC subsets in TDLNs (Fig. 3D). In the development of active immunotherapeutic strategies, much attention has been focused on $CD11b^+$ cDC-based vaccines that have failed to induce sufficient clinical efficacy (26), as pDCs are considered to be involved in the maintenance of antitumor tolerance (27) and to be inversely correlated with prognosis in patients with cancer (28, 29). However, pDC subsets can be pivotal players in TAA-specific antitumor immune responses by functioning as APCs (30) that use distinct MHC class II antigen-presentation molecules (31), leading to the effective priming of naïve $CD4^+$ T cells (32), and cross-present antigens with an efficiency comparable with $CD11b^+$ cDCs (33), implicating its potential as promising APCs for cancer immunotherapy. Indeed, imiquimod or CpG, a TLR9 agonist, reverted immunotolerant pDCs to antitumor pDCs (34), resulting in clinical antitumor effects (35, 36). Importantly, our results of *in vivo* experiments using pDC depletion and/or $IFNAR^{-/-}$ mice demonstrated the positive impact of the pDC subset and/or type I IFN signaling on the effective generation of GM-CSF–induced antitumor immunity (Fig. 3E and F). Thus, there may be a functional dichotomy in pDC biology between immune tolerance and antitumor phenotype, where their redirection is dependent on the tumor microenvironment.

Imiquimod, a TLR7 ligand, could be regarded as the most effective adjuvant among all approved immunomodulators based on the following: (i) topical imiquimod is currently FDA approved with a good safety profile; (ii) it potently activates APCs to release type I IFNs and Th1-skewing cytokines; and (iii) imiquimod treatment leads to CCL2-dependent recruitment of pDCs and their transformation into killer DCs (37). The underlying mechanism of substantial antitumor efficacy by the combined vaccination may be due to generation of functionally mature pDCs in TVSs and TDLNs (Fig. 5A and Supplementary Fig. S4). IFN-α, mainly produced from pDCs upon exposure to viruses via TLR7 or TLR9 (38), acts directly on memory T cells, which potentiate the antigen presentation and cross-priming capacities of $CD11b^+$ cDCs (39, 40). We detected $CD9^+$ pDCs, which produce abundant IFN-α (14), in TDLNs from mice injected with ir.LLC/SeV/GM cells (Fig. 5C and D). Furthermore, GM-CSF–sensitized pDCs expressed higher CD86 and Siglec-H (Fig. 5B), a regulator of pDC differentiation and $CD8^+$ T-cell responses (13, 41). Moreover, pDCs activated with GM-CSF plus imiquimod further enhanced the proliferation of $CD8^+$ T cells (Fig. 5F), indicating that GM-CSF–activated pDCs with or without imiquimod could serve as functional APCs to prime the potent generation of TAA-specific adaptive immunity. ELISPOT assay demonstrated that the number of IFN-γ–producing splenocytes from mice treated with irLLC/SeV/GM cells plus imiquimod was increased compared with control mice (data not shown). Indeed, depletion assays revealed that $CD4^+$ and $CD8^+$ T cells significantly contributed to the augmentation of the antitumor efficacy by combination GVAX therapy (Fig. 5G), thus reflecting the imiquimod-driven accelerated TAA-specific Th1 responses.

Although other researchers showed that the addition of imiquimod negates the antitumor efficacy of a GM-CSF–based vaccine (42), these conflicting results may stem from the difference in doses and administration schedule. It is noteworthy that the ability of imiquimod to potentiate the antitumor effect of GVAX therapy in two different types of cancers and in two different host strains might confirm the generality of our findings (Fig. 4C and D).

In conclusion, we, for the first time, elucidated that the beneficial roles of the pDCs and relevant type I IFN pathway in GM-CSF–induced antitumor immunity and that the combinational use of imiquimod with GVAX therapy produced synergistic antitumor effects, underscoring its potential as a promising approach for the treatment of cancer.

Disclosure of Potential Conflicts of Interest

K. Tani is a consultant/advisory board member. No potential conflicts of interest were disclosed by the other authors.

Authors' Contributions

Conception and design: M. Narusawa, H. Inoue, Y. Matsumura, K. Tani
Development of methodology: M. Narusawa, H. Inoue, Y. Matsumura, M. Inoue, M. Hasegawa
Acquisition of data (provided animals, acquired and managed patients, provided facilities, etc.): M. Narusawa, H. Inoue, C. Sakamoto, Y. Matsumura, A. Watanabe, K. Tani
Analysis and interpretation of data (e.g., statistical analysis, biostatistics, computational analysis): M. Narusawa, H. Inoue, Y. Matsumura, T. Inoue, S. Miyamoto
Writing, review, and/or revision of the manuscript: M. Narusawa, H. Inoue, A. Takahashi, Y. Tanaka, K. Takayama, T. Okazaki, Y. Nakanishi
Administrative, technical, or material support (i.e., reporting or organizing data, constructing databases): Y. Matsumura, T. Inoue, Y. Miura, M. Hasegawa, K. Tani
Study supervision: H. Inoue, Y. Matsumura, A. Takahashi, Y. Hijikata, T. Okazaki, K. Tani

Acknowledgments

The authors thank Michiyo Okada, Michiko Ushijima, Yosuke Yokota, and Haruka Nabeta for excellent technical assistance, and Kaori Yasuda and Atsushi Doi for performing the cDNA microarray analysis. The authors also thank Katsuaki Sato for valuable discussion.

Grant Support

This work was supported by JSPS KAKENHI grant number 21790773 and a grant for students through the Kyushu University Foundation research grant program.

The costs of publication of this article were defrayed in part by the payment of page charges. This article must therefore be hereby marked *advertisement* in accordance with 18 U.S.C. Section 1734 solely to indicate this fact.

Received September 5, 2013; revised February 5, 2014; accepted March 3, 2014; published OnlineFirst xx xx, xxxx.

References

1. Dranoff G, Jaffee E, Lazenby A, Golumbek P, Levitsky H, Brose K, et al. Vaccination with irradiated tumor cells engineered to secrete murine granulocyte-macrophage colony-stimulating factor stimulates potent, specific, and long-lasting anti-tumor immunity. Proc Natl Acad Sci U S A 1993;90:3539–43.
2. Tani K, Azuma M, Nakazaki Y, Oyaizu N, Hase H, Ohata J, et al. Phase I study of autologous tumor vaccines transduced with the GM-CSF gene in four patients with stage IV renal cell cancer in Japan: clinical and immunological findings. Mol Ther 2004;10:799–816.
3. Longo DL. New therapies for castration-resistant prostate cancer. N Engl J Med 2010;363:479–81.
4. Li HO, Zhu YF, Asakawa M, Kuma H, Hirata T, Ueda Y, et al. A cytoplasmic RNA vector derived from nontransmissible Sendai virus with efficient gene transfer and expression. J Virol 2000;74:6564–9.
5. Honda K, Yanai H, Negishi H, Asagiri M, Sato M, Mizutani T, et al. IRF-7 is the master regulator of type-I interferon-dependent immune responses. Nature 2005;434:772–7.
6. Inoue H, Iga M, Nabeta H, Yokoo T, Suehiro Y, Okano S, et al. Nontransmissible Sendai virus encoding granulocyte macrophage colony-stimulating factor is a novel and potent vector system for producing autologous tumor vaccines. Cancer Sci 2008;99:2315–26.
7. Yoneyama H, Matsuno K, Toda E, Nishiwaki T, Matsuo N, Nakano A, et al. Plasmacytoid DCs help lymph node DCs to induce anti-HSV CTLs. J Exp Med 2005;202:425–35.
8. Yokota Y, Inoue H, Matsumura Y, Nabeta H, Narusawa M, Watanabe A, et al. Absence of LTB4/BLT1 axis facilitates generation of mouse GM-CSF–induced long-lasting antitumor immunologic memory by enhancing innate and adaptive immune systems. Blood 2012;120:3444–54.
9. Sadler AJ, Williams BR. Interferon-inducible antiviral effectors. Nat Rev Immunol 2008;8:559–68.
10. Gilliet M, Cao W, Liu YJ. Plasmacytoid dendritic cells: sensing nucleic acids in viral infection and autoimmune diseases. Nat Rev Immunol 2008;8:594–606.
11. Colonna M, Trinchieri G, Liu YJ. Plasmacytoid dendritic cells in immunity. Nat Immunol 2004;5:1219–26.
12. Akira S, Hemmi H. Recognition of pathogen-associated molecular patterns by TLR family. Immunol Lett 2003;85:85–95.
13. Takagi H, Fukaya T, Eizumi K, Sato Y, Sato K, Shibazaki A, et al. Plasmacytoid dendritic cells are crucial for the initiation of inflammation and T cell immunity *in vivo*. Immunity 2011;35:958–71.
14. Bjorck P, Leong HX, Engleman EG. Plasmacytoid dendritic cell dichotomy: identification of IFN-alpha producing cells as a phenotypically and functionally distinct subset. J Immunol 2011;186:1477–85.
15. Shi L, Chen J, Zhong Q, Li M, Geng P, He J, et al. Inactivated Sendai virus strain Tianjin, a novel genotype of Sendai virus, inhibits growth of murine colon carcinoma through inducing immune responses and apoptosis. J Transl Med 2013;11:205.
16. Sumimoto H, Tani K, Nakazaki Y, Tanabe T, Hibino H, Hamada H, et al. GM-CSF and B7-1 (CD80) co-stimulatory signals co-operate in the induction of effective anti-tumor immunity in syngeneic mice. Int J Cancer 1997;73:556–61.
17. Wada H, Noguchi Y, Marino MW, Dunn AR, Old LJ. T cell functions in granulocyte/macrophage colony-stimulating factor deficient mice. Proc Natl Acad Sci U S A 1997;94:12557–61.
18. Yang H, Wei J, Zhang H, Lin L, Zhang W, He S. Upregulation of Toll-like receptor (TLR) expression and release of cytokines from P815 mast cells by GM-CSF. BMC Cell Biol 2009;10:37.
19. Barreda DR, Hanington PC, Belosevic M. Regulation of myeloid development and function by colony stimulating factors. Dev Comp Immunol 2004;28:509–54.
20. Kingston D, Schmid MA, Onai N, Obata-Onai A, Baumjohann D, Manz MG. The concerted action of GM-CSF and Flt3-ligand on *in vivo* dendritic cell homeostasis. Blood 2009;114:835–43.
21. Mausberg AK, Jander S, Reichmann G. Intracerebral granulocyte-macrophage colony-stimulating factor induces functionally competent dendritic cells in the mouse brain. Glia 2009;57:1341–50.
22. Daro E, Pulendran B, Brasel K, Teepe M, Pettit D, Lynch DH, et al. Polyethylene glycol-modified GM-CSF expands CD11b(high)CD11c(high) but notCD11b(low)CD11c(high) murine dendritic cells *in vivo*: a comparative analysis with Flt3 ligand. J Immunol 2000;165:49–58.
23. Esashi E, Wang YH, Perng O, Qin XF, Liu YJ, Watowich SS. The signal transducer STAT5 inhibits plasmacytoid dendritic cell development by suppressing transcription factor IRF8. Immunity 2008;28:509–20.
24. Schlitzer A, Loschko J, Mair K, Vogelmann R, Henkel L, Einwachter H, et al. Identification of CCR9$^-$ murine plasmacytoid DC precursors with plasticity to differentiate into conventional DCs. Blood 2011;117:6562–70.
25. Ghirelli C, Zollinger R, Soumelis V. Systematic cytokine receptor profiling reveals GM-CSF as a novel TLR-independent activator of human plasmacytoid predendritic cells. Blood 2010;115:5037–40.
26. Banchereau J, Palucka AK. Dendritic cells as therapeutic vaccines against cancer. Nat Rev Immunol 2005;5:296–306.